HHS Public Access

Author manuscript

Cell Rep. Author manuscript; available in PMC 2020 November 11.

Published in final edited form as:

Cell Rep. 2020 November 03; 33(5): 108341. doi:10.1016/j.celrep.2020.108341.

G9a Promotes Breast Cancer Recurrence through Repression of a Pro-inflammatory Program

Nathaniel W. Mabe[1], **Nina Marie G. Garcia**[1], **Shayna E. Wolery**[1], **Rachel Newcomb**[1], **Ryan C. Meingasner**[1], **Brittany A. Vilona**[1], **Ryan Lupo**[1], **Chao-Chieh Lin**[2,3], **Jen-Tsan Chi**[2,3], **James V. Alvarez**[1,4,*]

[1]Department of Pharmacology and Cancer Biology, Duke University, Durham, NC 27710, USA

[2]Department of Molecular Genetics and Microbiology, Duke University, Durham, NC 27710, USA

[3]Center for Genomic and Computational Biology, Duke University, Durham, NC 27710, USA

[4]Lead Contact

SUMMARY

Dysregulated gene expression is a common feature of cancer and may underlie some aspects of tumor progression, including tumor relapse. Here, we show that recurrent mammary tumors exhibit global changes in gene expression and histone modifications and acquire dependence on the G9a histone methyltransferase. Genetic ablation of G9a delays tumor recurrence, and pharmacologic inhibition of G9a slows the growth of recurrent tumors. Mechanistically, G9a activity is required to silence pro-inflammatory cytokines, including tumor necrosis factor (TNF), through H3K9 methylation at gene promoters. G9a inhibition induces re-expression of these cytokines, leading to p53 activation and necroptosis. Recurrent tumors upregulate receptor interacting protein kinase-3 (RIPK3) expression and are dependent upon RIPK3 activity. High RIPK3 expression renders recurrent tumors sensitive to necroptosis following G9a inhibition. These findings demonstrate that G9a-mediated silencing of pro-necroptotic proteins is a critical step in tumor recurrence and suggest that G9a is a targetable dependency in recurrent breast cancer.

Graphical Abstract

*Correspondence: james.alvarez@duke.edu.

AUTHOR CONTRIBUTIONS

N.W.M., N.M.G.G., S.E.W., R.N., R.C.M., and B.A.V. generated and analyzed data. R.N. and R.L. assisted with animal work. S.E.W., R.C.M., and B.A.V. assisted with generation of human cell line treatments. S.E.W. assisted with drug screening and biochemical analysis of p53 knockout. R.N. performed immune profiling. N.W.M. and J.V.A. wrote and edited the manuscript. J.V.A. supervised all work. All authors reviewed the manuscript.

SUPPLEMENTAL INFORMATION

Supplemental Information can be found online at https://doi.org/10.1016/j.celrep.2020.108341.

DECLARATION OF INTERESTS

The authors declare no competing interests.

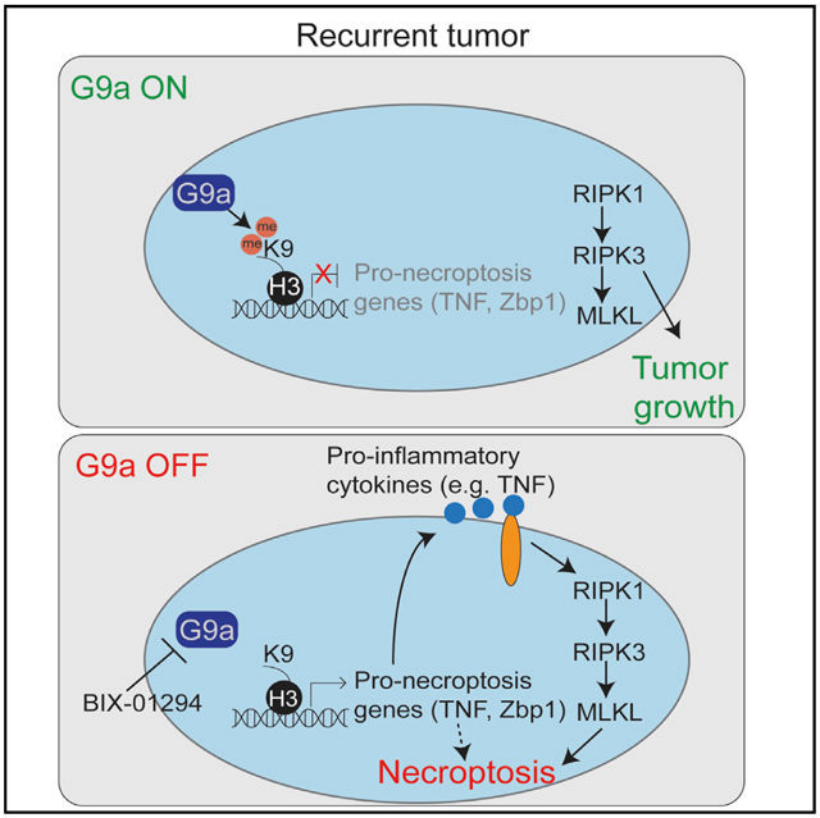

In Brief

Mabe et al. show that the histone methyltransferase G9a promotes breast cancer recurrence. They find that G9a functions to repress pro-inflammatory genes in recurrent tumors and demonstrate that elevated RIPK3 expression in recurrent tumor cells sensitizes these cells to necroptosis following G9a inhibition.

INTRODUCTION

It is increasingly appreciated that epigenetic dysregulation—that is, heritable changes in gene expression mediated by DNA methylation and posttranslational modifications on histones—can also contribute directly to tumor relapse and therapeutic resistance (Brien et al., 2016; Sharma et al., 2010). In cell culture models, epigenetic reprogramming can induce rapid and reversible resistance to targeted therapies and cytotoxic therapies (Shaffer et al., 2017; Sharma et al., 2010). In human cancer models, epigenetic modulation through EZH2 mediates adaptive resistance to chemotherapy in lung cancer (Gardner et al., 2017). Patient data also support the role of epigenetic dysregulation in breast cancer recurrence. Global histone lysine hypoacetylation and DNA hypomethylation are associated with poor prognosis in breast cancer (Elsheikh et al., 2009; Selli et al., 2019; Suzuki et al., 2009), and transcriptional reprogramming is a hallmark of chemoresistant, recurrent breast tumors (Yates et al., 2017). Together, these studies implicate epigenetic mechanisms in promoting drug resistance and breast tumor relapse. However, specific epigenetic alterations that

underlie breast cancer recurrence and therapeutic resistance have not been well defined and could identify clinically relevant targets in preventing or treating recurrent disease.

To gain insight into biological pathways driving tumor recurrence, we and others have used a genetically engineered mouse (GEM) mammary tumor model with conditional Her2 expression, which mimics key features of breast cancer recurrence in women (Alvarez et al., 2013; Goel et al., 2016; Moody et al., 2002). Administration of doxycycline (dox) to MMTV-rtTA;TetO-Her2/neu (MTB;TAN) mice induces Her2 expression in mammary epithelial cells, leading to the formation of Her2-driven adenocarcinomas. Dox withdrawal leads to tumor regression, but a small population of tumor cells can survive Her2 downregulation and persist as minimal, residual disease. After a latency of several months, those residual tumor cells spontaneously re-initiate proliferation and give rise to recurrent tumors. Importantly, those tumors recur independently of the Her2 oncogene, suggesting tumors have acquired Her2-independent bypass mechanisms for their growth, mirroring observations in HER2-discordant human breast cancers. Although previous studies using HER2-driven recurrence models have identified genetic alterations in some recurrent tumors, including *Met* amplification (Feng et al., 2014) and *Cdkn2a* deletions (Goel et al., 2016), not all tumors have a clear genetic basis for recurrence. We reasoned that a subset of recurrent tumors may leverage non-genetic mechanisms to adapt to and recur after HER2 withdrawal. Characterizing epigenetic and transcriptional profiles of primary and recurrent tumors could identify non-genetic mechanisms by which tumor cells survive Her2 downregulation and form recurrent tumors. In the current study, we used these GEM models to evaluate the contribution of epigenetic remodeling to breast cancer recurrence.

RESULTS

Tumor Recurrence Is Associated with Widespread Epigenetic Remodeling

To gain insight into epigenetic changes associated with tumor recurrence, we derived cell lines from three primary and five recurrent tumors arising in MTB/TAN mice (Alvarez et al., 2013; Mabe et al., 2018). Consistent with prior work showing that *Met* gene amplification is a common genetic escape mechanism after oncogene withdrawal (Feng et al., 2014; Liu et al., 2011), we found that two of the five recurrent tumor cells had amplification of the *Met* gene (Figures S1A and S1B). We reasoned that in recurrent tumor cells lacking *Met* amplification, tumor recurrence may, instead, be driven by epigenetic reprogramming.

To characterize epigenetic alterations in these tumors, we performed genome-wide chromatic immunoprecipitation sequencing (ChIP-seq) on primary cells (#1 and #2) and recurrent tumor cells (#1, #2, and #3). We evaluated histone marks H3K9ac and H3K4me3, which are commonly localized to actively transcribed genes, and the repressive histone mark H3K27me3, which is found at repressive heterochromatin (Wang et al., 2009). RNA polymerase II (RNApol2) was included to mark actively transcribed genes. Global analysis showed that each of the histone marks, as well as RNApol2, was enriched at the promoter and the transcription start site of active genes (Figure S1C). Differential binding (DiffBind) analysis for each histone modification showed that 29% of H3K4me3 peaks, 47% of H3K9ac peaks, and 18% of H3K27me3 peaks were differentially enriched in either primary or recurrent tumor cells, with recurrent cells having slightly more differential peaks than

primary cells (Figure 1A). Half of the RNApol2 peaks we identified were differentially enriched in either primary or recurrent cells, with approximately equal numbers enriched in each cohort (Figure 1A). Although most differential peaks were found at active gene regulatory elements, an increased number of peaks for H3K4me3, H3K9ac, and H3K27me3 in recurrent cell lines were located in intergenic regions (>5 kb distance from a transcriptional start site; Figure S1D), and there was a substantial overlap of these differential H3K4me3 and H3K9ac intergenic peaks with the enhancer marks H3K4me1 and H3K27ac from ENCODE (Figure S1E), suggesting that these intergenic peaks may represent newly acquired enhancers in recurrent tumor cells (Bradner et al., 2017).

We next compared the enrichment of these marks at individual gene promoters between primary and recurrent tumor cells. One group of genes was epigenetically repressed in recurrent tumor cells, with elevated enrichment of H3K9ac, H3K4me3, and RNApol2 and decreased enrichment of H3K27me3 at their promoters in primary tumor cells compared with recurrent tumor cells (Figure 1B). Conversely, genes that were epigenetically activated in recurrent tumor cells displayed the opposite pattern, with elevated H3K9ac, H3K4me, and RNApol2 and decreased H3K27me3 peaks (Figure 1B). These results demonstrate that tumor recurrence is associated with genome-wide epigenetic remodeling.

Tumor Recurrence Is Associated with Transcriptional Rewiring

We reasoned that the genome-wide alterations in histone modifications between primary and recurrent tumor were likely associated with gene expression changes. To address that, we performed RNA-sequencing (RNA-sequencing) on three primary tumor cell lines (#1, #2, and #3) and four recurrent tumor cell lines (#1, #2, #3, and #4). Primary and recurrent tumors exhibited global differences in gene expression (Figure 1C) and clustered into distinct groups by principal components analysis (Figure 1D). Interestingly, the Met-amplified recurrent line (#4) had a gene expression pattern distinct from both primary and non-Met amplified recurrent tumor cells (Figures 1C and 1D), suggesting that Met amplification represents a distinct mode of tumor recurrence. Differential gene expression analysis identified 3,467 genes upregulated in recurrent tumor cells and 3,920 genes upregulated in primary tumor cells (adjusted [adj.] $p < 0.05$) (Figure 1E). These gene expression changes were strongly correlated with alterations in histone modifications at the gene promoters (Figure S1F), indicating that recurrent tumors exhibit genome-wide transcriptional changes that are associated with epigenetic rewiring.

To identify specific transcriptional programs altered in recurrent tumors, we performed gene set enrichment analysis (GSEA). Recurrent tumors were highly enriched for an epithelial-to-mesenchymal transition (EMT), as we and others have previously described (Mabe et al., 2018; Moody et al., 2005), as well as two independent Myc signatures (Figure 1F). Interestingly, a recent study in triple-negative breast cancer reported that EMT and Myc signatures are enriched in drug-resistant breast cancers (Kim et al., 2018). A number of genes found in the chemoresistant gene set were also upregulated in recurrent tumors, including Col1a1, Myc, Psat1, Cox6c, and Gastp1.

A substantial proportion of genes in both primary and recurrent tumor cells had bivalent promoters, marked by both the repressive histone mark H3K27me3 and the active histone

mark H3K4me3 (Figure S1G). Alterations in the expression of genes with bivalent promoters have been implicated in chemoresistance and enhanced breast cancer tumorigenicity (Chaffer et al., 2013; Chapman-Rothe et al., 2013). Consistent with that, we found a number of genes that were silenced through bivalent histone modifications in primary tumors and transcriptionally activated in recurrent tumors, including Mycn, Prrx2, Twist2, and Zeb1. Conversely, we identified two pro-apoptotic proteins, Bik and Pawr, that were expressed in primary tumors and silenced by bivalent regulation in recurrent tumors (Figure S1G).

Recurrent Tumor Cells Are Dependent on G9a Methyltransferase Activity

We hypothesized that epigenetic remodeling may be functionally important for the survival and recurrence of tumor cells after oncogene withdrawal and that recurrent tumors may acquire unique epigenetic dependencies that are not present in the primary tumors. To explore that hypothesis, we performed a small-molecule screen, testing the effect of inhibitors targeting various epigenetic enzymes on primary and recurrent tumor cell viability (Table S1). Two primary (#1 and #2) and two recurrent (#1 and #2) tumor cell lines were treated with increasing doses of each inhibitor, and cell viability was measured (Figure 2A). To identify drugs that differentially inhibit the growth of primary and recurrent tumor cells, we calculated the difference in half-maximal inhibitory concentration (IC_{50}) for primary and recurrent tumor cells for each drug; values less than 0 correspond to drugs more potent against recurrent tumor cells. This analysis identified two drugs that were significantly more potent in recurrent cells, the G9a inhibitor BIX-01294 (IC_{50} difference = −0.88; 95% confidence interval [95% CI], −1.23 to −0.543) and the Aurora kinase inhibitor lestaurtinib (IC_{50} difference = −1.06 [95% CI, −1.47 to −0.665) (Figure 2B). Because we could not calculate an IC_{50} for nine compounds, we also evaluated the difference in maximal drug efficacy for each inhibitor between primary and recurrent cells (Figure 2C). Six drugs were significantly more efficacious in recurrent tumor cell lines (adj. $P < 0.05$), including a G9a inhibitor (BIX-01294), a JMJD3 inhibitor (GSKJ1), an EZH2 inhibitor (EPZ5687), a DOT1L inhibitor (SGC0946), an LSD1 inhibitor (GSKLSD1), and a BAZ2A/B inhibitor (GSK2801) (Figure 2C).

We focused on the G9a-inhibitor BIX-01294 because it was among the most potent and efficacious inhibitors in recurrent tumor cells as compared with primary tumor cells. G9a is a histone methyltransferase that heterodimerizes with the structurally related G9a-like protein (GLP) to catalyze mono- and dimethylation of H3K9 (Jenuwein, 2006; Jenuwein et al., 1998; Tachibana et al., 2005). H3K9me1 and H3K9me2 are associated with transcriptional silencing of genes in euchromatin, whereas H3K9me3—which is deposited by Setdb1 or Suv39H1—is associated with repressed genes in heterochromatin (Rice et al., 2003; Schultz et al., 2002; Wang et al., 2003). BIX-01294 inhibits G9a/GLP by competing for binding with the amino acids N-terminal of the substrate lysine residue (Chang et al., 2009). We confirmed that BIX-01294 selectively inhibits recurrent tumor cell growth by additional cell viability assays (Figures 2D and 2E). We next tested whether recurrent tumor cells are differentially sensitive to additional G9a inhibitors. Both UNC0638, a substrate-competitive inhibitor, and BRD4770, an *S*-adenosyl-methionine (SAM)-competitive inhibitor, selectively inhibited the growth of recurrent tumor cells (Figures 2F and 2G). The

reduction in H3K9me2 levels after BIX-01294 treatment was equivalent between primary and recurrent tumor cells (Figure S2A) and was similar to the reduction in bulk H3K9me2 levels that has previously been reported with BIX-01294 (Vedadi et al., 2011). H3K9me2 reductions were observed at the 300 nM and 1 μM concentrations (Figures S2B and S2C), which is in line with the IC_{50} values observed in recurrent tumor cells.

To assess whether the effect of G9a inhibitors on recurrent cell viability was mediated through on-target inhibition of G9a, we used CRISPR-Cas9 to knock out G9a in primary and recurrent tumor cell lines. Cells were infected with lentivirus expressing a control single-guide RNA (sgRNA) targeting the Rosa26 locus (sgNT) or one of two independent sgRNAs targeting G9a (sgG9a) (Figure 2H). G9a knockout significantly inhibited the growth of recurrent tumor cell lines, whereas primary tumor cells lines were unaffected (Figure 2I), providing genetic confirmation that recurrent tumor cells are dependent on G9a activity.

Finally, we asked whether Met-amplified recurrent tumors were also sensitive to G9a inhibitors. To address that, we tested the effect of BIX treatment on an expanded panel of three primary tumor cell lines and five recurrent tumor cell lines. Although the growth of all non-Met-amplified recurrent cell lines was inhibited by BIX, neither of the two Met-amplified cell lines (#4 and #5) was sensitive to BIX (Figures S2D and S2E), indicating that Met-amplified tumors are not dependent upon G9a activity. Taken together, these results suggest that a subset of recurrent tumors acquire a dependence upon G9a methyltransferase activity.

G9a Promotes Tumor Recurrence *In Vivo*

We measured G9a expression in an independent cohort of seven primary and seven recurrent MTB/TAN tumors. G9a has a long isoform (G9a long) and a short isoform (G9a short) generated by alternative splicing. There was a trend toward increased expression of the short isoform recurrent tumors and in recurrent tumor cell lines (Figures 3A, 3B, S2F, and S2G). Intriguingly, mRNA levels of G9a were not increased in recurrent tumors or recurrent tumor cells (Figures S2H and S2I), suggesting that increased G9a protein expression is not mediated through increased transcript levels.

The observation that recurrent tumors upregulate G9a and are dependent upon G9a activity suggested that G9a may promote the development of recurrent tumors. To test that directly, we used an orthotopic recurrence assay to determine whether G9a knockout in primary tumors affects the latency of tumor recurrence. Control or G9a-knockout cells were injected into the inguinal mammary gland of nude mice on dox to generate primary tumors. Primary tumors from control and G9a knockout cells formed with similar kinetics (Figures 3C and S2J) and primary tumors maintained G9a knockout (Figure 3D), consistent with our findings that G9a knockout does not affect primary tumor cell growth *in vitro*. Once primary tumors reached ~75 mm^3, dox was withdrawn to induce Her2 withdrawal and tumor regression, and mice were monitored for the formation of recurrent tumors. G9a knockout significantly delayed the time to recurrence ($p = 0.0006$, hazard ratio [HR] = 0.02 (95% CI, 0.08–0.50) for sgG9a#1; $p < 0.0001$, HR = 0.06 (95% CI: 0.02–0.16) for sgG9a#2) (Figure 3E). Interestingly, many recurrent tumors maintained G9a knockout (Figure S2K), suggesting that these tumors had bypassed the requirement for G9a activity. Given that Met-amplified

are not sensitive to G9a inhibition, we considered Met amplification as one potential bypass mechanism. Indeed, we found that a greater proportion of G9a knockout recurrent tumors had amplified Met as compared with control recurrent tumors (Figure S2L), although that did not reach statistical significance, likely because of the small sample size. Taken together, these data show that G9a promotes tumor recurrence after Her2 downregulation.

Next, we evaluated whether pharmacologic inhibition of G9a can inhibit the growth of existing tumors *in vivo*. Recurrent or primary tumor cells were injected orthotopically into the inguinal mammary glands of FVB mice to generate orthotopic tumors, and mice were treated with BIX-01294 (10 mg/kg, intraperitoneal [i.p.]) three times weekly for 2 weeks. Consistent with *in vitro* data, BIX administration significantly reduced tumor growth and tumor burden in recurrent tumor cells (Figures 3F and 3G). In contrast, primary tumor growth was not inhibited by BIX-01294 treatment, and in fact, BIX-treated primary tumors grew slightly faster than control tumors (Figures 3H and 3I). BIX treatment also slowed the growth of orthotopic recurrent tumors in athymic nude recipients (Figure S2M), suggesting that the effects of G9a inhibition do not require an adaptive immune system.

Finally, we asked whether overexpression of G9a in primary tumors could accelerate tumor recurrence. Primary tumor cells were transduced with a retrovirus expressing G9a or empty vector (Figure S2N) and orthotopically injected into mice. Control and G9a-expressing primary tumors formed with similar kinetics (data not shown). Dox was withdrawn to induce Her2 downregulation and tumor regression, and mice were monitored for the formation of recurrent tumors. G9a expression significantly accelerated the formation of recurrent tumors (Figure 3J), further indicating that G9a promotes tumor recurrence after Her2 downregulation.

Integrated Epigenetic and Transcriptional Analysis of G9a-Regulated Genes in Recurrent Tumors

We previously found that the pro-apoptotic protein Par-4 is silenced in recurrent tumors, and its re-expression induces cell death in these cells. Therefore, we considered the possibility that Par-4 upregulation following G9a inhibition might mediate cell death in recurrent tumor cells. However, Par-4 expression was not increased after treatment with BIX-01294 (Figure S3A), consistent with the findings from our previous work showing that H3K9me2 levels at the Par-4 promoter were not elevated in recurrent tumor cells. This suggests that the effects of G9a inhibition on recurrent tumor cell viability are not mediated through upregulation of Par-4.

We next explored the mechanistic basis for the dependence of recurrent tumors on G9a activity by identifying genes whose expression is directly regulated by G9a specifically in recurrent tumor cells. To do that, we first performed RNA-seq on primary and recurrent tumor cells treated with BIX-01294 for 16 h. Importantly, this early timepoint precedes the induction of cell death in response to BIX-01294 treatment. Because Met-amplified recurrent tumors were not sensitive to G9a inhibition, we focused on gene expression changes induced by G9a inhibition in non-Met amplified recurrent tumor cells.

G9a inhibition led to only modest changes in gene expression in primary tumor cells (Figure 4A; Table S2). In contrast, G9a inhibition induced widespread changes in gene expression in recurrent tumor cells (Figure 4A). We examined genes that were more significantly altered by BIX treatment in recurrent tumor cells as compared with primary tumor cells; 306 genes were differentially upregulated after BIX treatment in recurrent tumor cells, and 137 genes were differentially downregulated after BIX treatment (Figure 4A). Among the differentially upregulated genes were genes known to induce cell cycle arrest and cell death, including p21, Gadd45a, and Ccng2 (Figures 4B and S3B). Importantly, most genes whose expression changed after G9a inhibition were upregulated, consistent with G9a's role in repressing genes through H3K9 methylation.

We next overlapped genes upregulated after G9a inhibition in recurrent tumor cells with H3K9 ChIP-seq data to generate a list of genes likely to be directly regulated by G9a through H3K9 methylation. Because we were unable to successfully perform ChIP-seq to identify H3K9me2 peaks (data not shown), we considered a reduction in H3K9 acetylation in recurrent tumor cells as a proxy for increased H3K9 methylation. We identified 342 genes that (1) had lower H3K9 acetylation in recurrent tumor cells as compared with primary tumor cells, and (2) were upregulated after G9a inhibition specifically in recurrent tumor cells (Figure 4C; Table S3). We used ChIP-qPCR to assess H3K9me2 levels at the promoter of 10 of these putative G9a target genes and found that nine of 10 genes had elevated levels of H3K9me2 in recurrent tumor cells, suggesting that reduction in H3K9ac is a suitable surrogate for increased H3K9 methylation (Figure S3C). These 342 genes represent putative direct targets of G9a in recurrent tumor cells whose re-expression may mediate cell death after G9a inhibition.

Gene ontology analysis revealed that these G9a targets are enriched for genes involved in regulation of inflammatory responses, cytokine production, and tumor necrosis factor (TNF) signaling (Figure 4D). Examination of specific genes revealed that the pro-inflammatory cytokines TNF, interleukin 23a (IL-23a), and Cxcl2 were all induced after G9a inhibition in recurrent tumor cells (Figures S4A–S4C). Consistent with that, GSEA showed enrichment of a TNF-nuclear-factor-κB (NF-κB) signature and an inflammatory response signature in recurrent cells treated with BIX-01294 (Figures 4E and 4F). Taken together, these results indicate that G9a directly represses an inflammatory gene expression program in recurrent tumor cells and raise the possibility that upregulation of pro-inflammatory genes may contribute to cell death in recurrent tumor cells following G9a inhibition.

A G9a Signature Is Associated with Increased Risk of Recurrence in Human Breast Cancer

We next examined whether elevated G9a activity is associated with increased risk of recurrence in human breast cancer using the G9a gene expression signature described above to identify tumors with high G9a activity. Tumors with low expression of these G9a signature genes were considered to have a high G9a signature. We found that patients whose tumors had a high G9a signature (i.e., low expression of G9a targets) had significantly shorter recurrence-free survival (Figure 4G) (Ringnér et al., 2011). Interestingly, this association was especially strong in HER2-enriched and luminal B breast tumors, many of

which have *HER2* gene amplification. Taken together, these results suggest that high G9a activity is associated with increased risk of recurrence in breast cancer.

G9a-Dependent Silencing of TNF Is Required for Recurrent Tumor Cell Survival

To investigate whether upregulation of pro-inflammatory cytokines contributes to cell death after G9a inhibition, we focused our attention on TNF. TNF was among the most differentially induced cytokines after BIX-01294 treatment in recurrent versus primary tumor cells, and the TNF promoter had reduced H3K9 acetylation in recurrent as compared with primary tumor cells (Figure 5A). Further, G9a has been reported to regulate TNF in other models (Li et al., 2018). TNF can induce tumor-cell-specific cell death in certain cancer cell types and lineages, including breast cancer (Burow et al., 1998; Wang and Lin, 2008). We first tested whether G9a regulates TNF through H3K9 methylation in our model. At baseline, TNF expression was slightly lower in recurrent tumor cells as compared with primary tumor cells (Figure S3A). G9a inhibition led to a 4- to 50-fold increase in TNF levels in recurrent cells, but only induced modest changes in TNF levels in primary cells, as measured by qRT-PCR (Figure 5B). Further, H3K9me2 levels at the TNF promoter were significantly greater in recurrent tumor cells as compared with primary tumor cells (Figure 5C) and were reduced after BIX-01294 treatment (Figure 5D), confirming that G9a promotes H3K9 methylation at the TNF promoter. We next asked whether TNF selectively inhibits recurrent tumor cell growth. Treatment with recombinant TNF led to a marked decrease in the growth of recurrent tumor cells, but had only a modest effect on primary tumor cells (Figures 5E and S4D). Similar results were obtained in long-term colony formation assays (Figure 5F). However, blocking TNF signaling with an anti-TNF antibody was not sufficient to reverse BIX-mediated cell death in recurrent tumor cells, suggesting that other pro-inflammatory factors may function in concert with TNF to mediate cell death in response to G9a inhibition (Figure S4E). Taken together, these results demonstrate that G9a directly silences pro-inflammatory cytokines, including TNF, in recurrent tumor cells, and that re-activation of these genes mediates the anti-tumor effects of G9a inhibition in recurrent tumors.

Given that G9a inhibition induces expression of pro-inflammatory genes in recurrent tumor cells, we examined whether G9a inhibition is associated with alterations in the tumor immune microenvironment. To evaluate that, we performed immune cell profiling on recurrent and primary orthotopic tumors treated with BIX-01294 using markers for leukocytes, monocytes, macrophages, and T cells. G9a inhibition did not significantly alter any of the immune cell populations in recurrent (Figure S4F) or primary tumors (data not shown). Although those results do not rule out the possibility that G9a inhibition affects the tumor immune microenvironment, they suggest that G9a inhibition slows the growth of recurrent tumors through tumor cell-intrinsic pathways, consistent with the observation that BIX treatment inhibits recurrent tumor cell growth *in vitro* (see Figure 2) and in immunocompromised mice (see Figures S2K and S2L).

G9a Inhibition Leads to Induction of p53 Targets and p53-Dependent Cell Death

RNA-seq analysis revealed that a p53 signature was enriched following G9a inhibition (Figure S5A), so we explored the function of the p53 pathway in recurrent tumor cells'

response to G9a inhibition. Western blot analysis showed that p53 protein is expressed in all primary and recurrent tumor cell lines (Figure S5B) and sequencing of p53 identified no mutations in either primary or recurrent tumor cell lines (data not shown). qPCR analysis showed that the canonical p53 targets Cdkn1a (p21) and Gadd45a were significantly upregulated in BIX-treated, recurrent tumor cell lines (Figure S5C), suggesting that the p53 signaling axis is intact in recurrent tumor cells and that p53 targets genes are upregulated in response to G9a inhibitors.

To determine whether p53 is required to mediate cell death in response to G9a inhibition, we knocked out p53 in recurrent tumor cell lines using CRISPR/Cas9 (Figure S5D). p53 knockout markedly reduced the induction of p21 and Gadd45a after BIX treatment in recurrent tumor cell lines (Figure S5E), but the induction of these genes was not completely reduced after p53 knockdown, suggesting that G9a may regulate their expression in part through p53-independent mechanisms. Significantly, p53 knockout resulted in an approximately 3-fold shift in the potency of BIX-01294 in recurrent tumor cell line #1 (IC_{50} for sgNT 168 nM; IC_{50} for sgp53 613 nM) and an approximately 2-fold shift in recurrent cell lines #2 (IC_{50} for sgNT 120 nM; IC_{50} for sgp53 248 nM) and #3 (IC_{50} for sgNT 476 nM; IC_{50} for sgp53 867 nM) (Figure S5F). Consistent with that, Annexin V staining showed that p53 knockout partially decreased cell death following BIX-01294 treatment (Figure S5G). Taken together, these results indicate that p53 partially contributes to cell death after G9a inhibition, suggesting the presence of both p53-dependent and -independent cell death pathways.

G9a Inhibition Induces Necroptotic Cell Death

The results described above indicate that G9a inhibition leads to upregulation of pro-inflammatory cytokines, and one such cytokine, TNF, is sufficient to reduce cell viability in recurrent cells. Because TNF can induce both apoptotic and necroptotic cell death pathways (Laster et al., 1988; Nikoletopoulou et al., 2013), we next sought to define the mode of cell death following G9a inhibition. G9a inhibition led to a marked increase in Annexin V staining only in recurrent tumor cells (Figures 6A and 6B). Annexin V binds to phosphatidylserine (PS) on the outer leaflet of the plasma membrane, and PS flipping is a marker of both apoptosis and necroptosis. To differentiate between these cell death pathways, we examined molecular markers specific for each cell death pathway. The apoptotic markers cleaved caspase-3 and cleaved poly(ADP-ribose) polymerase (PARP) were not induced after BIX-01294 treatment (Figure 6C). Instead, BIX-01294 treatment led to a marked increase in phosphorylation of S345 of MLKL (Figure 6C), which is a marker of necroptosis and is associated with induction of necroptosis during TNF-mediated cell death (Rodriguez et al., 2016). Consistent with that, we found that a necroptosis gene expression signature containing 141 necroptosis-associated genes (Table S4) (Callow et al., 2018; Chen et al., 2018a; Hitomi et al., 2008; Zhu et al., 2018) was enriched after G9a inhibition in recurrent tumor cells (Figure 6D). These results indicate that G9a inhibition leads to necroptotic cell death in recurrent tumor cells.

To evaluate whether induction of necroptosis is necessary for BIX-mediated cell death, we pre-treated recurrent tumor cell lines with the RIPK1 inhibitor Necrostatin-1 (Nec-1). Nec-1

partially rescued cell viability after BIX treatment in three recurrent tumor cell lines (Figure 6E) and decreased the proportion of Annexin-V-positive cells after BIX-01294 (Figure 6F). The finding that Nec-1 partially reversed cell death induced by G9a inhibition but a blocking antibody against TNF did not (Figure S4E) suggested that G9a inhibition can induce necroptosis through multiple, redundant pathways. We, therefore, examined the necroptosis gene signature (Figure 6D) to identify potential additional mediators of necroptosis after G9a inhibition. RNA-seq analysis revealed that, in addition to TNF, TLR3 was modestly upregulated and Zbp1 was substantially upregulated after G9a inhibition (Table S2). qRT-PCR analysis confirmed that BIX-01294 treatment led to a 2-fold to 6-fold upregulation of Zbp1 in recurrent tumor cells (Figure S5H). TLR3, a member of the Toll-like receptor family, and Zbp1, a cytosolic nucleic acid sensor, are two alternate pathways that can lead to the induction of necroptosis (Grootjans et al., 2017) and represent additional candidate pathways that may mediate the induction of necroptosis following G9a inhibition.

In light of our previous observation that p53 contributes to cell death following G9a inhibition, we next addressed the role of p53 in BIX-induced necroptosis. p53 knockout cells failed to induce MLKL phosphorylation after BIX-01294 treatment (Figure 6G). Consistent with that, qPCR analysis indicated that TNF upregulation was blunted in p53 knockout cells treated with BIX, suggesting that p53 activity is required for TNF expression (Figure S5I). Taken together, our data suggest that p53 is required for TNF-dependent necroptosis in recurrent tumor cells.

Recurrent Tumor Cells Are Dependent on RIPK3

To understand why recurrent tumor cells are sensitized to undergo necroptosis after G9a inhibition, we evaluated the expression of critical intermediates in the necroptosis pathway. Necroptosis is triggered through a multiprotein complex called the necrosome, consisting of RIPK1 and RIPK3 (Newton, 2015), which acts to phosphorylate and activate MLKL, ultimately leading to cell membrane disruption and necroptosis (Weinlich et al., 2017). Conversely, caspase-8 can inhibit necroptosis at least in part through cleaving RIPK1 and RIPK3 (O'Donnell et al., 2011). We examined expression of RIPK1, RIPK3, caspase-8, and MLKL in primary and recurrent tumor cells (Figures 7A and S6A–S6C). RNA sequencing revealed that RIPK1 and MLKL were expressed at similar levels between primary and recurrent tumor cells (Figures S6B and S6C). In contrast, we observed a 2-fold decrease in caspase-8 expression and a nearly 1,000-fold increase in RIPK3 expression in recurrent tumor cells (Figures 7A and S6A). qPCR and western blotting confirmed that RIPK3 was dramatically upregulated in recurrent tumor cells relative to primary tumor cells (Figures 7B and 7C). Intriguingly, Met-amplified recurrent tumor cell lines did not upregulate RIPK3, consistent with the finding that these cells are resistant to G9a inhibition (Figures 7B and 7C). To test whether RIPK3 is sufficient to induce sensitivity to TNF-induced necroptosis, we engineered primary tumor cells expressing RIPK3. RIPK3 expression in primary tumor cells increased their sensitivity to TNF-induced cell death (Figures S6D and S6E). These results suggest that upregulation of RIPK3 in recurrent tumor cells underlies, at least in part, their sensitivity to both G9a inhibition and TNF treatment.

RIPK3 is traditionally thought to function as a tumor suppressor (Vucur et al., 2013). Consistent with that, RIPK3 expression is silenced in >85% of patients with breast cancer (Koo et al., 2015). In contrast to its tumor-suppressive function, several recent reports have suggested that RIPK3 may drive tumor growth (Hänggi et al., 2017; Liu et al., 2016; Seifert et al., 2016). Given that RIPK3 is highly expressed in recurrent, and not primary, tumor cells, we hypothesized that recurrent tumor cells may depend on RIPK3 activity. To test that hypothesis, we tested the effect of pharmacologic inhibition of RIPK3 on tumor cell growth; inhibitors against RIPK1 and MLKL were included as controls. Although the RIPK1 inhibitor Nec-1 and the MLKL inhibitor necrosulfonamide (NSA) had minimal effects on recurrent tumor cell viability, the RIPK3 inhibitor GSK'872 pro-foundly inhibited recurrent tumor cell viability in two cell lines (Figures 7D–7F). Further, all three recurrent cell lines exhibited decreased cell viability in response to genetic knockdown of RIPK3 with two independent short hairpin RNAs (shRNAs) (Figures 7G and S6F). Taken together, these data suggest that elevated RIPK3 expression promotes recurrent tumor cell growth, and that this can be pharmacologically targeted.

Finally, we investigated whether G9a also regulates cell viability and inflammatory cytokine expression in human breast cancer cell lines. We measured the response of 24 breast cancer cell lines to increasing concentrations of BIX-01294; the normal mammary epithelial cell line MCF10A was included as a control (Figures S7A and S7B). Only SKBR3 cells had an IC_{50} for BIX less than 1 μM, consistent with previous reports that SKBR3 cells are sensitive to G9a inhibition (Figures S7A and S7B) (Kim et al., 2013). Similar to recurrent mouse tumors, SKBR3 cells had elevated expression of RIPK3 as compared with MCF7 and MCF10A cell lines, both of which are resistant to G9a inhibition (Figure S7C). Analysis of a wide panel of breast cancer cell lines from the Cancer Cell Line Encyclopedia revealed that, although most cell lines had low or undetectable levels of RIPK3, consistent published reports (Koo et al., 2015), ~25% of those cell lines had appreciable RIPK3 expression (Figure S7D). The frequency of RIPK3 expression was independent of breast cancer subtype or p53 mutational status. Further, BIX treatment induced robust expression of TNF in multiple breast cancer cell lines (Figure S7E). These data suggest that G9a can regulate TNF expression in a range of human breast cancer cell lines.

DISCUSSION

In the current study, we used a GEM model of Her2-driven breast cancer to examine mechanisms underlying Her2-independent tumor recurrence. We found that a subset of recurrent tumors underwent widespread epigenetic reprogramming and displayed profound changes in gene expression as compared with primary tumors. These epigenetic changes were associated with an acquired dependency of recurrent tumors on the histone methyltransferase G9a. Genetic knockout of G9a delayed tumor recurrence, and pharmacologic inhibition of G9a prevented the growth of recurrent tumors. Conversely, ectopic expression of G9a accelerated tumor recurrence. These results were mirrored in human patients with breast cancer, where a G9a signature was associated with decreased recurrence-free survival, especially in HER2-amplified tumors. Mechanistically, G9a was required in recurrent tumors to silence pro-inflammatory genes. Inhibition of G9a led to the re-expression of pro-inflammatory genes and the induction of necroptotic cell death.

Surprisingly, recurrent tumors had dramatically upregulated expression of the essential necroptosis protein RIPK3. RIPK3 activity was both required for recurrent tumor cell growth and sensitized recurrent tumor cells to necroptosis. Taken together, we found that G9a-dependent epigenetic reprogramming promotes breast cancer recurrence and identified a G9a-RIPK3 pathway as a targetable collateral vulnerability in recurrent breast cancer (Figure 7H).

RNA-seq and ChIP-seq analysis revealed that recurrent tumors had profound transcriptional and epigenetic differences from primary tumors. Results from an epigenetic inhibitor screen suggested that recurrent tumors had acquired new epigenetic dependencies as compared with primary tumors. Together, this strongly suggests that epigenetic remodeling is functionally important for tumor recurrence. Indeed, inhibition of G9a delayed tumor recurrence and slowed recurrent tumor growth. Although the results presented here focus on G9a, it is possible that other chromatin-modifying enzymes are also functionally important for tumor recurrence. Consistent with that, we found that recurrent tumor cells had acquired new H3K9ac, H3K4me3, and RNApol2 peaks at intergenic regions. Although the mechanisms underlying these epigenetic changes remain unknown, our results suggest that epigenetic remodeling is a major feature of tumor recurrence, and this remodeling is associated with an acquired dependence on the G9a histone methyltransferase.

By integrating global gene expression and ChIP-seq data, we found that G9a directly regulates the expression of a set of pro-inflammatory genes, including TNF, in recurrent tumor cells. Treatment with TNF by itself was sufficient to inhibit the growth of recurrent, but not primary, tumor cells. Mechanistically, the selective sensitivity of recurrent tumor cells to TNF was due to recurrent tumor cells upregulating the essential necroptosis kinase RIPK3. Expression of RIPK3 sensitized primary tumor cells to TNF-induced cell death, whereas blocking necroptosis partially reversed recurrent tumor cell death in response to G9a inhibition. RIPK3 is traditionally thought to function as a tumor suppressor, and its expression is often silenced in breast cancers (Koo et al., 2015), and so its upregulation in recurrent tumors was unexpected. However, a handful of recent reports have identified a pro-tumorigenic function for RIPK3 that is independent of necroptosis (Newton, 2015; Seifert et al., 2016). Consistent with that, we found that RIPK3 was required for the growth of recurrent tumor cells, although the mechanistic basis for that requirement remains unknown. Taken together, this suggests a model in which RIPK3 upregulation is both required for recurrent tumor cell growth and sensitizes those cells to stimuli that induce necroptosis, including TNF. According to that model, the dependence of recurrent tumors for G9a activity is due, at least in part, to the requirement for recurrent tumor cells to silence TNF expression. This is an example of the concept of collateral sensitivity, in which a resistance pathway—in this case, high RIPK3 expression—results in enhanced sensitivity to a secondary pathway, G9a.

A number of previous studies have found that inhibitors targeting G9a (Casciello et al., 2017; Tu et al., 2018) or the H3K27 methyltransferase Ezh2 (Chen et al., 2018b; Gardner et al., 2017) are effective in various cancers, either alone or in combination with chemotherapy. However, more-recent studies have suggested that the effects of epigenetic inhibitors can be more complex, and are likely to be context dependent. For instance, two recent studies have

shown that inhibition of G9a drives the formation of tumors with more-aggressive, stem-like phenotypes (Avgustinova et al., 2018; Rowbotham et al., 2018). In the study by Avgustinova et al. (2018), G9a knockout delayed the formation of carcinogen-induced skin tumors, but once G9a-knockout tumors formed they were more aggressive, with higher levels of genomic instability and more frequent p53 loss. These results suggest that G9a can have context-dependent roles in regulating tumor progression and underscore the importance of crosstalk between G9a and p53 in dictating the net result of G9a inhibition.

In conclusion, our results demonstrate that tumor recurrence is associated with widespread epigenetic reprogramming and acquired dependence on the histone methyltransferase G9a. These findings elucidate a role for G9a in silencing pro-necroptotic inflammatory cytokines in cancer. Finally, these observations suggest that strategies designed to target G9a may have clinical utility to improve survival in patients diagnosed with recurrent breast cancer.

Limitations of Study

One limitation of the present study is the lack of evidence that TNF-induced necroptosis mediates cell death in recurrent tumors after G9a inhibition *in vivo*. Although we demonstrate the importance of necroptotic cell death following G9a inhibition *in vitro* (Figures 6E and 6F), similar experiments performed *in vivo* would strengthen the proposed mechanism. Definitive proof that necroptosis mediates tumor cell death and the reduction in tumor growth in response to G9a inhibition *in vivo* remains an important goal. Furthermore, although we show that TNF is sufficient to induce necroptotic cell death in recurrent tumor cells *in vitro*, TNF upregulation was not necessary for necroptosis after G9a inhibition because blocking TNF signaling with a neutralizing antibody did not prevent necroptosis after G9a inhibition. Future work should focus on identifying the pathways that are required for necroptosis after G9a inhibition; upregulation of the nucleic acid sensor Zbp1 is one plausible candidate.

A second outstanding question concerns the net effect of the TNF pathway in the recurrence of HER2-positive breast cancers. Previous work from our laboratory found that TNF has *pro-tumor* effects in primary tumors from this Her2-driven breast tumor model (Walens et al., 2019). We showed that Her2 inhibition leads to upregulation of TNF, which functions in an autocrine manner to induce expression of a suite of chemoattractant cytokines, including CCL5. CCL5 expression, in turn, promotes recurrence through altering the tumor immune microenvironment. In contrast, in the current study, we find that TNF has *anti-tumor* effects in recurrent tumor cells through inducing necroptotic cell death. These differing consequences of TNF on primary versus recurrent tumors highlight the frequently opposing effects of this pleiotropic cytokine on tumor growth (Balkwill, 2009). There are at least two differences in how TNF acts on primary, as compared with recurrent, tumors that can explain these opposing effects. Although, in primary tumors, the pro-tumor effects of TNF are mediated by the microenvironment, in recurrent tumors TNF inhibits tumor growth through tumor-cell-intrinsic effects. Second, the anti-tumor effects of TNF on recurrent tumors are dependent on those cells being primed to undergo necroptosis because of high expression of RIPK3. As we show in Figures 5E and 5F, TNF has no effect on the growth of primary tumor cells *in vitro* in the absence of the tumor microenvironment. In sum, the net effect of

TNF on tumor growth in this model is dependent on both the tumor microenvironment and the gene expression context of the tumor cells themselves. This has important implications for treating patients with breast cancer because the consequences of an anti-TNF therapy would depend on both the tumor microenvironment and the expression of necroptotic genes in the tumor cells themselves. Given that anti-TNF therapies may differentially affect primary versus recurrent tumor growth *in vivo*, future work with TNF inhibitors will be required to dissect the net effect of the TNF pathway on tumor recurrence.

STAR★METHODS

RESOURCE AVAILABILITY

Lead contact—Further information and requests for resources and reagents should be directed to and will be fulfilled by the Lead Contact, James Alvarez (James.Alvarez@duke.edu).

Materials availability—Plasmids generated in this study are available upon request.

Data and code availability—Complete RNA- and ChIP-sequencing data are available online using National Center for Biotechnology Information's Short Read Archive (SRA) under project accession number SRA: PRJNA505839.

EXPERIMENTAL MODEL AND SUBJECT DETAILS

Mice—Animal care and all animal experiments were performed with the approval of and in accordance with Duke University IACUC guidelines (A199-17-08). MMTV-rtTA;TetO-Her2/neu (MTB;TAN) and TetO-Her2/neu (TAN) mice are on an FVB background. Wild-type FVB mice were purchased from Jackson laboratory. Nu/nu mice were obtained from the Duke University Breeding Core. Mice were fed a standard chow diet and housed under barrier conditions with 12-hour light/dark cycles. Female mice were used for all studies. Dox was administered to MTB;TAN mice at 6-weeks of age. For orthotopic tumor studies, cells were injected into the fourth mammary gland of recipient mice at 6-weeks of age.

Orthotopic Recurrence Assays—Female nude mice were randomized into cages and maintained on 2 mg/mL doxycycline for two days prior to orthotopic injection. 1×10^6 primary tumors cells (#2) expressing Cas9 and either sgNT, sgG9a#1, or sgG9a#2 were injected bilaterally into the fourth mammary gland of nude mice (n = 10 per sgRNA, n = 30 mice total). Tumor size was determined by caliper measurement at least three times a week until tumors reached ~75 mm^3. Two mice (n = 4 tumors) were sacrificed with primary tumors for downstream biochemical analysis. The remaining 8 mice were removed from dox to initiate tumor regression. Mice were palpated at least three times a week to monitor for tumor recurrence (~75mm^3). Recurrence-free survival was determined using Kaplan-Meier survival analysis and differences in recurrence were assessed using the Mantel-Cox log-rank test.

***In vivo* BIX administration—**200,000 recurrent tumor cells (line #3) or 500,000 primary tumor cells (line #2) were injected bilaterally into the inguinal (fourth) mammary gland of

FVB or TAN female mice, respectively. TAN mice are used as hosts for primary tumor cells because these mice are tolerized to the luciferase protein (data not shown). Female mice were used to ensure the appropriate mammary gland microenvironment for growth of mammary tumors. Mice were randomized to receive vehicle (n = 5 mice) or BIX treatment (n = 5 mice; 10 mg/kg) by intraperitoneal injections three times a week for two weeks starting one day after tumor cell injections. Tumors size was determined by caliper measurements daily until mouse sacrifice. Mice were sacrificed once tumors reached 250 mm^3. Tumor volume was calculated using the equation $((\pi \times length \times width^2) / 6)$. Tumor growth curves were compared between treatment groups by repeated-measures, two-way ANOVA (time × treatment) and Sidak's multiple comparisons test. Tumor AUC was calculated using the equation $[(vol_1 + vol_2)/2] \times (day_2 - day_1)$. Tumor burden was compared between treatment groups by unpaired Student's t test.

Tissue culture—Primary and recurrent tumor cell lines were derived and grown from MTB;TAN mice as previously described (Alvarez et al., 2013; Mabe et al., 2018). All human cell lines (SKBR3, AU565, BT-474, HCC1500, HCC1428, T-47D, MCF-7, HCC1937, HCC1143, MDA-MB-231, MCF10A, MDA-MB-134, HCC1395, MDA-MB-361, HCC38, BT-483, HCC1954, MDA-MB-436, BT-549, HCC1569, ZR-75–1, UACC-812, BT-20, MDA-MB-157, HCC1419, HS578T) were obtained from Duke University Cell Culture Facility and cultured according to ATCC medium recommendations. Cell lines were authenticated and tested for mycoplasma according to standard procedures at Duke University. Cell lines were used within 6 months of receipt.

METHOD DETAILS

Plasmids and viral transduction—To knock out expression of G9a or p53, Cas9 was stably infected in cell lines using a lentiviral construct encoding lentiCas9-Blast (a gift from Feng Zhang, Addgene #52962). The single-guide RNAs targeting G9a and p53 listed in the Key Resources Table were cloned into lentiGuide-Puro (a gift from Feng Zhang, Addgene #52963). For knockdown of RIPK3, lentiviral shRNAs listed in the Key Resources Table were purchased from Dharmacon. For G9a overexpression, a cDNA encoding the long isoform of G9a was purchased from Dharmacon (clone ID:6822432) and cloned into the pBabe-Puro plasmid using the following primers: forward primer 5′-GTTAGGATCCATGGCGGCGGCGGCGGGAGC-3′, and reverse primer 5′-GTTAGAATTCTTAAGAGTCCTCAGGTGTTG-3′.

Retrovirus was produced by transfecting AmphoPhoenix packaging cells with the retroviral expression construct (National Gene Vector Repository). Lentivirus was produced by transfection of HEK293T cell line with psPAX2 and the lentiviral expression construct. Sodium butyrate (1 mM) was added 24 and 48 h after transfection to boost viral titers. Viral supernatant was collected 48 and 72 h post-transfection, filtered, and used to transduce target cells in the presence of 4 μg/mL polybrene. Cells were selected in media containing puromycin (2 μg/mL for primary tumor cells; 4 μg/mL for recurrent tumor cells) and/or blasticidin (5 μg/mL).

Small-molecule screen—Tumor cells from primary #1, primary #2, recurrent #1, and recurrent #2 were plated at 1,500 cells / well on 96-well plates and allowed overnight to attach. Cells were treated with 8 increasing concentrations (vehicle, 10 nM, 30 nM, 100 nM, 300 nM, 1 μM, 3 μM, 10 μM) of each drug in biological triplicate for 60 h. Each well was normalized to the average of vehicle-treated control wells corresponding to the cell line. Cell viability was determined using the CellTiterGlo kit according to the manufacturer's instructions. The IC_{50} and SEM were determined for each primary and recurrent cohort by combining all 6 biological replicates. The difference in IC_{50} and 95% confidence interval were determined by inputting log[IC_{50}] and SEM for each cohort into a web-based tool available at https://www.graphpad.com/quickcalcs/errorProp1/?Format=SEM.

The following drugs were purchased and utilized as part of the CaymanChem epigenetics screening library (#11076): Cl^- Amidine, PFI-1, JQ1, GSK2801, SGC0946, N-oxalylglycine, OTX015, JIB01, RG108, Rucaparib, GSKJ1, UNC1215, lestaurtinib, BIX-01294, EPZ5687, GSKLSD1, PFI2, Lomeguatrib, PFI3, C646, Daminozide, AGK2, SGCCBP. Additional drugs included, UNC-0638 (Tocris), BIX-01294 (Tocris), BRD4770 (SelleckChem), Necrostatin-1 (SelleckChem), GSK'872 (SelleckChem), necrosulfonamide (SelleckChem), and Z-VAD-FMK (SelleckChem). Drugs were solubilized per manufacturer recommendations and utilized at concentrations stated within the text. Matching vehicle controls were used for each experiment.

Cell growth and cell viability assays—Concentration-response curves were determined by plating 1,000 cells from primary and recurrent tumor cell lines in triplicate on a 96-well plate. Cells were allowed to grow overnight prior to 48 h treatment with increasing concentrations of the following drugs: BIX-01294, UNC0638, BRD4770, Nec-1, GSK'872, and Necrosulfonamide. Cell viability was measured by CellTiterGlo kit. A single IC_{50} with standard error was calculated by nonlinear regression for each cohort and significance between cohorts determined by Student's unpaired t test. Concentration-response curves were generated in GraphPad Prism 7 software.

Cell growth kinetics following G9a knockout in primary (#1 and #2) and recurrent (#1 and #2) tumor cells was determined by plating 1,000 cells in triplicate on a 96-well plate. Cell viability was determined using CellTiterGlo on days 1, 3, and 5 post-plating. Relative cell viability was determined by calculating the ratio of luminescence on days 3 and 5 as compared to day 1.

For crystal violet staining, primary or recurrent tumor cells were plated onto 6-well plates (60,000 cells/well) and then treated with 2 μM BIX-01294 for 48 h. For measurement of cell viability following RIPK3 knockdown, tumor cells were infected with lentivirus expressing one of two shRNAs targeting RIPK3 (shRipk#1 TRCN0000022534, shRIPK3#2 TRCN0000022538) and selected in puromycin. Four days after infection, 50,000 tumor cells were plated onto 10-cm plates and grown for 7–9 days until confluency. Plates were washed with PBS and stained with 0.5% crystal violet for 5 min. Excess crystal violet was rinsed with water and plates scanned.

For short-term cell viability following TNF administration, 1,000 cells from each primary (#1, #2, and #3) and recurrent (#1, #2, #3) tumor cell lines were plated in triplicate on 96-well plates and treated for 72 h with 10 ng/mL TNF or 0.1% BSA vehicle control. Cell viability was determined using CellTiterGlo. Long-term colony formation assays were performed by plating 1,500 cells on 10-cm plates and treating with 10 ng/mL TNF or vehicle control for 7 days. Plates were washed with PBS and stained with 0.5% crystal violet. Plates were analyzed on Li-Cor Odyssey®. For cell viability assays with necrostatin-1, 1,000 tumor cells from recurrent (#1, #2, and #3) lines were plated in triplicate and treated for 16 h with 300 nM BIX-01294 alone or in combination with 30 μM Necrostatin-1.

Immunoblotting and qRT-PCR—Immunoblotting and qRT-PCR was performed as previously described (Mabe et al., 2018). For histone blots, histones were extracted from cell pellets by the protocol found at https://www.abcam.com/protocols/histone-extraction-protocol-for-western-blot. Primary antibodies used for immunoblotting and gene probes used for qRT-PCR are listed in the Key Resources Table.

Copy Number Assay—DNA was extracted using the Allprep kit according to manufacturer instructions and diluted to 5 ng/μL. 7.5 μL master mix was generated for each well in the following ratios: 5 μL genotyping Taqman mastermix 0.5 μL of each the Met and Tfrc copy number probes found in the Key Resources Table, and 1.5 μL of water. 2.5 μL was added to master mix for a total of 10 μL reactions in each well. Samples were run on a CFX384 Real-Time PCR Detection System (BioRad). Met Ct values were normalized to Tfrc using ΔΔCt and compared to normal mouse DNA.

In-cell western—7,500 tumor cells (Primary #1, Primary #2, Recurrent #1 and Recurrent #2) were plated in duplicate on a black, clear-bottom 96-well plate. Cells were treated for 48 h with increasing concentrations of BIX-01294 and then fixed with 3.7% formaldehyde for 20 min at room temperature, washed with PBS, and permeabilized with 0.1% Triton X-100 in PBS. Cells were blocked for 1 h with a 3% goat serum, 1% BSA, 0.1% Triton X-100 solution, prior to overnight incubation of primary antibodies listed in the Key Resources Table. Secondary antibodies AlexaFluor® 680 and IRDye®800 were diluted 1:2000 in PBST and were incubated on cells for 1 h. Plates were imaged with a Li-Cor Odyssey® infrared imaging system (Li-Cor Biosciences). Mean fluorescence of each well was analyzed in ImageStudio Lite software (Li-Cor) and the signal ratio determined by dividing the H3K9me2 signal by the Histone H3 signal.

Flow Cytometry—150,000 tumor cells (Prim #1, Prim #2, Rec #1 and Rec#3) were plated on 6-cm plates and treated for 16 h with 1 μM BIX-01294 or vehicle control. To test the requirement for necroptosis, recurrent lines #1 or #3 were plated in biological triplicate and treated with vehicle, or 750 nM BIX-01294 with or without 30 μM Necrostatin-1. After treatment, cells were trypsinized and washed with PBS. Cell pellets were resuspended into 100 uL of Annexin-binding buffer (Life Technologies) containing 1:20 Annexin V-AlexaFluor® 488 and propidium iodide and incubated for 20 min. Samples were diluted with 400 μL of additional Annexin-binding buffer and passed through a 40 μm filter.

Samples were excited with a 488 nm laser and 10,000 events were analyzed on a BD FACSCanto II flow cytometer. Data were analyzed using FlowJo software.

Immune profiling—Orthotopic tumors were manually chopped and digested in a buffer containing: EBSS media 1X collagenase (300 Units/mL) / hyaluronidase (100 Units/mL), 2% FBS 0.1 mg/mL gentamycin, and 1X penicillin (2000 Units/mL) / streptomycin (2000 Units/mL) for 3 h at 37°C. Tumors were washed twice with media, and then incubated in a digestion buffer of 5 Units/mL dispase and 0.1 mg/mL DNase I Cell pellets were incubated in ACK lysis buffer for 5 min and rinsed twice in FACS buffer. Tumor cells were strained through a 40 micron filter and resuspended to 1×10^7 cells / mL in FACS staining buffer. 1×10^6 of cells were blocked with 2 μL of CD16/CD32 antibody for 10 min on ice. The cells were then incubated for 30 min with antibodies appropriate for cell panels of interest (leukocytes, macrophages, or T cells) (Key Resources Table) Samples were rinsed twice with staining buffer prior to analysis on BD FACSCanto II flow cytometer and data were analyzed using FlowJo software.

ChIP- and RNA-sequencing—Chromatin immunoprecipitation was performed as previously described with antibodies and primers found in the Key Resources Table and Table S5 (Mabe et al., 2018).

Chip-Seq analysis—Following immunoprecipitation, DNA was quantified using the fluorometric quantitation Qubit 2.0 system (ThermoFisher Scientific) and fragment size confirmed with Agilent Tapestation. DNA libraries were prepared using Kapa BioSystem HyperPrep Library Kit for compatibility with Illumina sequencing. Unique indexes were added to each sample. Resulting libraries were cleaned using SPRI beads, quantified with Qubit 2.0 and Agilent Bioanalyzer, and pooled into equimolar concentrations. Pools were sequenced on Illumina Hiseq 4000 sequencer with 50 bp single reads at a depth of ~55 million reads per sample. Fastq reads underwent strict quality control processing with the TrimGalore package to remove low quality bases and trim adaptor sequences. Reads passing quality control were mapped to mm10 version of the mouse genome using the Bowtie short read aligner (Langmead et al., 2009). Duplicate reads were filtered and peaks were called with the MACS2 peak-calling algorithm using default parameters, except for H3K27me3 peaks which were called using ‘broad peak’ settings (Zhang et al., 2008). Following sequencing, differential binding analysis was completed with DiffBind software on standard settings (Ross-Innes et al., 2012). Differentially bound sites were annotated with ChIPseeker (Yu et al., 2015) and annotatr (Cavalcante and Sartor, 2017) packages. Enhancer regions were based on Fantom5 classifications. Bam alignment files were converted into bigwig files by binning reads into 100bp segments. Global enrichment plots and heatmap visuals for H3K4me3, H3K9ac, K3K27me3, and RNApol2 at the top 100 most differentially enriched RNApol2 peaks in primary and recurrent cohorts were generated using deepTools2 software (Ramírez et al., 2016). The number of overlapping ChIP-seq peaks with at least one base pair shared was determined with ChIPpeakAnno (Zhu et al., 2010). Publicly available H3K4me1 and H3K27ac ChIP-seq data for mouse embryonic fibroblasts were obtained from ENCODE (via Bing Ren, Ludwig Institute for Cancer Research) and accessed via GEO

numbers GSM769028 and GSM1000139, respectively (ENCODE Project Consortium, 2012).

RNA sequencing—RNA was extracted using the RNeasy kit (QIAGEN) and concentrations quantified using Qubit 2.0 and Agilent Bioanalyzer. cDNA libraries were prepared with the Kapa stranded mRNA kit. Pooled sample libraries were sequenced on HiSeq 4000 (Illumina) sequencer to 50 bp single reads at ~25–30 million read depth per sample. Fastq files were assessed for quality control with FastQC software. Raw sequencing reads were then trimmed of low quality base pairs and adapters with Trim Galore! Processed sequencing reads were aligned to the mm10 genome with STAR ultrafast universal RNA-seq aligner (Dobin et al., 2013). The number of transcript counts per gene were counted on the reverse strand with featureCounts software and organized into a count matrix for passing through differential gene expression analysis with DESeq2 software (Love et al., 2014). Of note, recurrent tumor cell line #2 and primary tumor cell line #3 were completed as a separate batch, and were corrected by adding the batch number as an additional variable. PCA analysis was produced using limma and ggplot2 package, and heatmaps were generated with pheatmap package in R (v3.5.2) software. Gene ontology for differential gene expression between primary and recurrent tumor cell lines was determined with clusterProfiler software (Yu et al., 2012). For GSEA analysis, genes were pre-ranked based on topics of interest (i.e., genes differentially expressed in recurrent tumor cell lines or genes upregulated following BIX administration) and input into desktop GSEA software (Broad Institute).

To determine whether the magnitude of gene expression is significantly altered between primary and recurrent tumor cells, the DEseq2 model was designed using Batch + Cell_Line + Condition + Cell_Line:Condition. Significant differences in the magnitude of induction was determined by an adjusted *P value* of < 0.05. Recurrent tumor cell line #4 was excluded from these analyses, as we were interested in gene expression alterations specific to recurrent tumor cell lines that were sensitive to G9a inhibition. Significantly altered genes from the analysis were labeled in color on the scatterplot of gene expression changes specific to recurrent cells (y axis) and primary cells (x axis) in R software using ggplot2 software.

For heatmap generation of significantly altered genes with BIX treatment, $\log_2$ gene expression was median-centered within each cohort (i.e., recurrent and primary) to eliminate baseline gene expression differences between primary and recurrent cohorts. Each row was Z-score normalized and input into ‘pheatmap’ software. Genes were clustered according to ‘complete’ method.

Integrated RNA- and ChIP-sequencing—Genes that were significantly upregulated with BIX in recurrent tumor cell lines #1, #2, and #3 by RNA sequencing (P. adj. < 0.05 versus primary tumor cell lines #1, #2, and #3) were overlapped with gene promoters significantly depleted (P adj. < 0.05) of H3K9ac in recurrent tumor cell lines #1, #2, and #3 relative to primary tumor cell lines #1 and #2 by ChIP-sequencing. Dot plot of overlapped data were generated in GraphPad Prism 8 software. Gene ontology of these genes was determined by clusterProfiler package (Yu et al., 2012). This G9a-regulated gene set was

input into online software (available at: http://co.bmc.lu.se/gobo/gsa.pl) to determine human distant metastasis-free survival based on a gene set. Settings for this analysis were set for distant metastasis-free survival (DMFS) for all tumors censored at 10 days and divided into 3 quantiles (Ringnér et al., 2011). Shown are plots for Luminal B and Her2-enriched tumors. A high G9a signature was determined by low global expression of G9a-regulated genes.

QUANTIFICATION AND STATISTICAL ANALYSIS

Western blots show representative results from at least two independent experiments. Gene expression analysis show results from a single representative experiment and are shown as the mean ± the SEM. Two-tailed Student's t test was used for statistical analyses between two groups. One- or two-way ANOVA with Sidak's multiple comparisons test was used to compare statistics across multiple groups. Fisher's exact test was used to evaluate significance between categorical (i.e., Met amplification) data. Differences in survival were determined by Mantel-Cox log-rank test. A p value of < 0.05 was considered significant. Specific details about the number replicates are found within the Figure Legends.

Supplementary Material

Refer to Web version on PubMed Central for supplementary material.

ACKNOWLEDGMENTS

We thank So Young Kim and the Duke Functional Genomics Core for the generation and validation of single-guide RNAs targeting G9a and p53; David Corcoran for assistance in the interpretation of ChIP-sequencing data; and Nicolas Devos from the Duke Sequencing and Genomics Technologies Core for acquisition of RNA- and ChIP-sequencing reads. We thank members of the Alvarez laboratory, including Andrea Walens for assistance with mammary gland injections, Ashley DiMarco for technical assistance with flow cytometry, and Doug Fox for the generation of Cas9-expressing tumor cells. This work was funded by the National Cancer Institute under award numbers R01CA208042 (to J.V.A.), F31CA220851 (to N.W.M.), and F31CA239421 (to R.N.) as well as the American Cancer Society under award 132556-RSG-18-130-CCG (to J.V.A.) and by startup funds from the Duke Cancer Institute, the Duke University School of Medicine, and the Whitehead Foundation (to J.V.A.).

REFERENCES

Alvarez JV, Pan TC, Ruth J, Feng Y, Zhou A, Pant D, Grimley JS, Wandless TJ, Demichele A, and Chodosh LA; I-SPY 1 TRIAL Investigators (2013). Par-4 downregulation promotes breast cancer recurrence by preventing multinucleation following targeted therapy. Cancer Cell 24, 30–44. [PubMed: 23770012]

Avgustinova A, Symeonidi A, Castellanos A, Urdiroz-Urricelqui U, Solé-Boldo L, Martín M, Pérez-Rodríguez I, Prats N, Lehner B, Supek F, and Benitah SA (2018). Loss of G9a preserves mutation patterns but increases chromatin accessibility, genomic instability and aggressiveness in skin tumours. Nat. Cell Biol 20, 1400–1409. [PubMed: 30455462]

Balkwill F (2009). Tumour necrosis factor and cancer. Nat. Rev. Cancer 9, 361–371. [PubMed: 19343034]

Bradner JE, Hnisz D, and Young RA (2017). Transcriptional addiction in cancer. Cell 168, 629–643. [PubMed: 28187285]

Brien GL, Valerio DG, and Armstrong SA (2016). Exploiting the epigenome to control cancer-promoting gene-expression programs. Cancer Cell 29, 464–476. [PubMed: 27070701]

Burow ME, Weldon CB, Tang Y, Navar GL, Krajewski S, Reed JC, Hammond TG, Clejan S, and Beckman BS (1998). Differences in susceptibility to tumor necrosis factor alpha-induced apoptosis among MCF-7 breast cancer cell variants. Cancer Res. 58, 4940–4946. [PubMed: 9810003]

Callow MG, Watanabe C, Wickliffe KE, Bainer R, Kummerfield S, Weng J, Cuellar T, Janakiraman V, Chen H, Chih B, et al. (2018). CRISPR whole-genome screening identifies new necroptosis regulators and RIPK1 alternative splicing. Cell Death Dis. 9, 261. [PubMed: 29449584]

Casciello F, Al-Ejeh F, Kelly G, Brennan DJ, Ngiow SF, Young A, Stoll T, Windloch K, Hill MM, Smyth MJ, et al. (2017). G9a drives hypoxia-mediated gene repression for breast cancer cell survival and tumorigenesis. Proc. Natl. Acad. Sci. USA 114, 7077–7082. [PubMed: 28630300]

Cavalcante RG, and Sartor MA (2017). annotatr: genomic regions in context. Bioinformatics 33, 2381–2383. [PubMed: 28369316]

Chaffer CL, Marjanovic ND, Lee T, Bell G, Kleer CG, Reinhardt F, D'Alessio AC, Young RA, and Weinberg RA (2013). Poised chromatin at the ZEB1 promoter enables breast cancer cell plasticity and enhances tumorigenicity. Cell 154, 61–74. [PubMed: 23827675]

Chang Y, Zhang X, Horton JR, Upadhyay AK, Spannhoff A, Liu J, Snyder JP, Bedford MT, and Cheng X (2009). Structural basis for G9a-like protein lysine methyltransferase inhibition by BIX-01294. Nat. Struct. Mol. Biol, 16, 312–317. [PubMed: 19219047]

Chapman-Rothe N, Curry E, Zeller C, Liber D, Stronach E, Gabra H, Ghaem-Maghami S, and Brown R (2013). Chromatin H3K27me3/H3K4me3 histone marks define gene sets in high-grade serous ovarian cancer that distinguish malignant, tumour-sustaining and chemo-resistant ovarian tumour cells. Oncogene 32, 4586–4592. [PubMed: 23128397]

Chen D, Tong J, Yang L, Wei L, Stolz DB, Yu J, Zhang J, and Zhang L (2018a). PUMA amplifies necroptosis signaling by activating cytosolic DNA sensors. Proc. Natl. Acad. Sci. USA 115, 3930–3935. [PubMed: 29581256]

Chen L, Alexe G, Dharia NV, Ross L, Iniguez AB, Conway AS, Wang EJ, Veschi V, Lam N, Qi J, et al. (2018b). CRISPR-Cas9 screen reveals a MYCN-amplified neuroblastoma dependency on EZH2. J. Clin. Invest 128, 446–462. [PubMed: 29202477]

Dobin A, Davis CA, Schlesinger F, Drenkow J, Zaleski C, Jha S, Batut P, Chaisson M, and Gingeras TR (2013). STAR: ultrafast universal RNA-seq aligner. Bioinformatics 29, 15–21. [PubMed: 23104886]

Elsheikh SE, Green AR, Rakha EA, Powe DG, Ahmed RA, Collins HM, Soria D, Garibaldi JM, Paish CE, Ammar AA, et al. (2009). Global histone modifications in breast cancer correlate with tumor phenotypes, prognostic factors, and patient outcome. Cancer Res. 69, 3802–3809. [PubMed: 19366799]

ENCODE Project Consortium (2012). An integrated encyclopedia of DNA elements in the human genome. Nature 489, 57–74. [PubMed: 22955616]

Feng J, Liu T, Qin B, Zhang Y, and Liu XS (2012). Identifying ChIP-seq enrichment using MACS. Nat Protoc. 7, 1728–1740. 10.1038/nprot.2012.101. [PubMed: 22936215]

Feng Y, Pan TC, Pant DK, Chakrabarti KR, Alvarez JV, Ruth JR, and Chodosh LA (2014). SPSB1 promotes breast cancer recurrence by potentiating c-MET signaling. Cancer Discov. 4, 790–803. [PubMed: 24786206]

Gardner EE, Lok BH, Schneeberger VE, Desmeules P, Miles LA, Arnold PK, Ni A, Khodos I, de Stanchina E, Nguyen T, et al. (2017). Che-mosensitive relapse in small cell lung cancer proceeds through an EZH2-SLFN11 axis. Cancer Cell 31, 286–299. [PubMed: 28196596]

Goel S, Wang Q, Watt AC, Tolaney SM, Dillon DA, Li W, Ramm S, Palmer AC, Yuzugullu H, Varadan V, et al. (2016). Overcoming therapeutic resistance in HER2-positive breast cancers with CDK4/6 inhibitors. Cancer Cell 29, 255–269. [PubMed: 26977878]

Grootjans S, Vanden Berghe T, and Vandenabeele P (2017). Initiation and execution mechanisms of necroptosis: an overview. Cell Death Differ. 24, 1184–1195. [PubMed: 28498367]

Hänggi K, Vasilikos L, Valls AF, Yerbes R, Knop J, Spilgies LM, Rieck K, Misra T, Bertin J, Gough PJ, et al. (2017). RIPK1/RIPK3 promotes vascular permeability to allow tumor cell extravasation independent of its necroptotic function. Cell Death Dis. 8, e2588. [PubMed: 28151480]

Hitomi J, Christofferson DE, Ng A, Yao J, Degterev A, Xavier RJ, and Yuan J (2008). Identification of a molecular signaling network that regulates a cellular necrotic cell death pathway. Cell 135, 1311–1323. [PubMed: 19109899]

Jenuwein T (2006). The epigenetic magic of histone lysine methylation. FEBS J. 273, 3121–3135. [PubMed: 16857008]

Jenuwein T, Laible G, Dorn R, and Reuter G (1998). SET domain proteins modulate chromatin domains in eu- and heterochromatin. Cell. Mol. Life Sci 54, 80–93. [PubMed: 9487389]

Kim Y, Kim YS, Kim DE, Lee JS, Song JH, Kim HG, Cho DH, Jeong SY, Jin DH, Jang SJ, et al. (2013). BIX-01294 induces autophagy-associated cell death via EHMT2/G9a dysfunction and intracellular reactive oxygen species production. Autophagy 9, 2126–2139. [PubMed: 24322755]

Kim C, Gao R, Sei E, Brandt R, Hartman J, Hatschek T, Crosetto N, Foukakis T, and Navin NE (2018). Chemoresistance evolution in triple-negative breast cancer delineated by single-cell sequencing. Cell 173, 879–893.e813. [PubMed: 29681456]

Koo GB, Morgan MJ, Lee DG, Kim WJ, Yoon JH, Koo JS, Kim SI, Kim SJ, Son MK, Hong SS, et al. (2015). Methylation-dependent loss of RIP3 expression in cancer represses programmed necrosis in response to chemotherapeutics. Cell Res. 25, 707–725. [PubMed: 25952668]

Langmead B, Trapnell C, Pop M, and Salzberg SL (2009). Ultrafast and memory-efficient alignment of short DNA sequences to the human genome. Genome Biol. 10, R25. [PubMed: 19261174]

Laster SM, Wood JG, and Gooding LR (1988). Tumor necrosis factor can induce both apoptic and necrotic forms of cell lysis. J. Immunol 141, 2629–2634. [PubMed: 3171180]

Li H, Yao Q, Mariscal AG, Wu X, Hüulse J, Pedersen E, Helin K, Waisman A, Vinkel C, Thomsen SF, et al. (2018). Epigenetic control of IL-23 expression in keratinocytes is important for chronic skin inflammation. Nat. Commun 9, 1420. [PubMed: 29650963]

Liao Y, Smyth GK, and Shi W (2019). The R package Rsubread is easier, faster, cheaper and better for alignment and quantification of RNA sequencing reads. Nucleic Acids Res. 47, e47 10.1093/nar/gkz114. [PubMed: 30783653]

Liu P, Cheng H, Santiago S, Raeder M, Zhang F, Isabella A, Yang J, Semaan DJ, Chen C, Fox EA, et al. (2011). Oncogenic PIK3CA-driven mammary tumors frequently recur via PI3K pathway-dependent and PI3K pathway-independent mechanisms. Nat. Med 17, 1116–1120. [PubMed: 21822287]

Liu X, Zhou M, Mei L, Ruan J, Hu Q, Peng J, Su H, Liao H, Liu S, Liu W, et al. (2016). Key roles of necroptotic factors in promoting tumor growth. Oncotarget 7, 22219–22233. [PubMed: 26959742]

Love MI, Huber W, and Anders S (2014). Moderated estimation of fold change and dispersion for RNA-seq data with DESeq2. Genome Biol. 15, 550. [PubMed: 25516281]

Mabe NW, Fox DB, Lupo R, Decker AE, Phelps SN, Thompson JW, and Alvarez JV (2018). Epigenetic silencing of tumor suppressor Par-4 promotes chemoresistance in recurrent breast cancer. J. Clin. Invest 128, 4413–4428. [PubMed: 30148456]

Moody SE, Sarkisian CJ, Hahn KT, Gunther EJ, Pickup S, Dugan KD, Innocent N, Cardiff RD, Schnall MD, and Chodosh LA (2002). Conditional activation of Neu in the mammary epithelium of transgenic mice results in reversible pulmonary metastasis. Cancer Cell 2, 451–461. [PubMed: 12498714]

Moody SE, Perez D, Pan TC, Sarkisian CJ, Portocarrero CP, Sterner CJ, Notorfrancesco KL, Cardiff RD, and Chodosh LA (2005). The transcriptional repressor Snail promotes mammary tumor recurrence. Cancer Cell 8, 197–209. [PubMed: 16169465]

Newton K (2015). RIPK1 and RIPK3: critical regulators of inflammation and cell death. Trends Cell Biol. 25, 347–353. [PubMed: 25662614]

Nikoletopoulou V, Markaki M, Palikaras K, and Tavernarakis N (2013). Crosstalk between apoptosis, necrosis and autophagy. Biochim. Biophys. Acta 1833, 3448–3459. [PubMed: 23770045]

O'Donnell MA, Perez-Jimenez E, Oberst A, Ng A, Massoumi R, Xavier R, Green DR, and Ting AT (2011). Caspase 8 inhibits programmed necrosis by processing CYLD. Nat. Cell Biol 13, 1437–1442. [PubMed: 22037414]

Ramírez F, Ryan DP, Grüning B, Bhardwaj V, Kilpert F, Richter AS, Heyne S, Dündar F, and Manke T (2016). deepTools2: a next generation web server for deep-sequencing data analysis. Nucleic Acids Res. 44 (W1), W160–W165. [PubMed: 27079975]

Rice JC, Briggs SD, Ueberheide B, Barber CM, Shabanowitz J, Hunt DF, Shinkai Y, and Allis CD (2003). Histone methyltransferases direct different degrees of methylation to define distinct chromatin domains. Mol. Cell 12, 1591–1598. [PubMed: 14690610]

Ringnér M, Fredlund E, Häkkinen J, Borg Å, and Staaf J (2011). GOBO: gene expression-based outcome for breast cancer online. PLoS ONE 6, e17911. [PubMed: 21445301]

Rodriguez DA, Weinlich R, Brown S, Guy C, Fitzgerald P, Dillon CP, Oberst A, Quarato G, Low J, Cripps JG, et al. (2016). Characterization of RIPK3-mediated phosphorylation of the activation loop of MLKL during necroptosis. Cell Death Differ. 23, 76–88. [PubMed: 26024392]

Ross-Innes CS, Stark R, Teschendorff AE, Holmes KA, Ali HR, Dunning MJ, Brown GD, Gojis O, Ellis IO, Green AR, et al. (2012). Differential oestrogen receptor binding is associated with clinical outcome in breast cancer. Nature 481, 389–393. [PubMed: 22217937]

Rowbotham SP, Li F, Dost AFM, Louie SM, Marsh BP, Pessina P, Anbarasu CR, Brainson CF, Tuminello SJ, Lieberman A, et al. (2018). H3K9 methyltransferases and demethylases control lung tumor-propagating cells and lung cancer progression. Nat. Commun 9, 4559. [PubMed: 30455465]

Schultz DC, Ayyanathan K, Negorev D, Maul GG, and Rauscher FJ 3rd. (2002). SETDB1: a novel KAP-1-associated histone H3, lysine 9-specific methyltransferase that contributes to HP1-mediated silencing of euchromatic genes by KRAB zinc-finger proteins. Genes Dev. 16, 919–932. [PubMed: 11959841]

Seifert L, Werba G, Tiwari S, Giao Ly NN, Alothman S, Alqunaibit D, Avanzi A, Barilla R, Daley D, Greco SH, et al. (2016). The necrosome promotes pancreatic oncogenesis via CXCL1 and Mincle-induced immune suppression. Nature 532, 245–249. [PubMed: 27049944]

Selli C, Turnbull AK, Pearce DA, Li A, Fernando A, Wills J, Renshaw L, Thomas JS, Dixon JM, and Sims AH (2019). Molecular changes during extended neoadjuvant letrozole treatment of breast cancer: distinguishing acquired resistance from dormant tumours. Breast Cancer Res. 21, 2. [PubMed: 30616553]

Shaffer SM, Dunagin MC, Torborg SR, Torre EA, Emert B, Krepler C, Beqiri M, Sproesser K, Brafford PA, Xiao M, et al. (2017). Rare cell variability and drug-induced reprogramming as a mode of cancer drug resistance. Nature 546, 431–435. [PubMed: 28607484]

Sharma SV, Lee DY, Li B, Quinlan MP, Takahashi F, Maheswaran S, McDermott U, Azizian N, Zou L, Fischbach MA, et al. (2010). A chromatin-mediated reversible drug-tolerant state in cancer cell subpopulations. Cell 141, 69–80. [PubMed: 20371346]

Suzuki J, Chen YY, Scott GK, Devries S, Chin K, Benz CC, Waldman FM, and Hwang ES (2009). Protein acetylation and histone deacetylase expression associated with malignant breast cancer progression. Clin. Cancer Res 15, 3163–3171. [PubMed: 19383825]

Tachibana M, Ueda J, Fukuda M, Takeda N, Ohta T, Iwanari H, Sakihama T, Kodama T, Hamakubo T, and Shinkai Y (2005). Histone methyltransferases G9a and GLP form heteromeric complexes and are both crucial for methylation of euchromatin at H3-K9. Genes Dev. 19, 815–826. [PubMed: 15774718]

Tu WB, Shiah YJ, Lourenco C, Mullen PJ, Dingar D, Redel C, Tamachi A, Ba-Alawi W, Aman A, Al-Awar R, Cescon DW, Haibe-Kains B, Arrowsmith CH, Raught B, Boutros PC, and Penn LZ (2018). MYC interacts with the G9a histone methyltransferase to drive transcriptional repression and tumorigenesis. Cancer Cell 34, 579–595.e578. [PubMed: 30300580]

Vedadi M, Barsyte-Lovejoy D, Liu F, Rival-Gervier S, Allali-Hassani A, Labrie V, Wigle TJ, Dimaggio PA, Wasney GA, Siarheyeva A, et al. (2011). A chemical probe selectively inhibits G9a and GLP methyltransferase activity in cells. Nat. Chem. Biol 7, 566–574. [PubMed: 21743462]

Vucur M, Reisinger F, Gautheron J, Janssen J, Roderburg C, Cardenas DV, Kreggenwinkel K, Koppe C, Hammerich L, Hakem R, et al. (2013). RIP3 inhibits inflammatory hepatocarcinogenesis but promotes cholestasis by controlling caspase-8- and JNK-dependent compensatory cell proliferation. Cell Rep. 4, 776–790. [PubMed: 23972991]

Walens A, DiMarco AV, Lupo R, Kroger BR, Damrauer JS, and Alvarez JV (2019). CCL5 promotes breast cancer recurrence through macrophage recruitment in residual tumors. eLife 8, e43653. [PubMed: 30990165]

Wang X, and Lin Y (2008). Tumor necrosis factor and cancer, buddies or foes? Acta Pharmacol. Sin 29, 1275–1288. [PubMed: 18954521]

Wang H, An W, Cao R, Xia L, Erdjument-Bromage H, Chatton B, Tempst P, Roeder RG, and Zhang Y (2003). mAM facilitates conversion by ESET of dimethyl to trimethyl lysine 9 of histone H3 to cause transcriptional repression. Mol. Cell 12, 475–487. [PubMed: 14536086]

Wang Z, Zang C, Cui K, Schones DE, Barski A, Peng W, and Zhao K (2009). Genome-wide mapping of HATs and HDACs reveals distinct functions in active and inactive genes. Cell 138, 1019–1031. [PubMed: 19698979]

Weinlich R, Oberst A, Beere HM, and Green DR (2017). Necroptosis in development, inflammation and disease. Nat. Rev. Mol. Cell Biol 18, 127–136. [PubMed: 27999438]

Yates LR, Knappskog S, Wedge D, Farmery JHR, Gonzalez S, Martincorena I, Alexandrov LB, Van Loo P, Haugland HK, Lilleng PK, Gundem G, Gerstung M, Pappaemmanuil E, Gazinska P, Bhosle SG, Jones D, Raine K, Mudie L, Latimer C, Sawyer E, Desmedt C, Sotiriou C, Stratton MR, Sieuwerts AM, Lynch AG, Martens JW, Richardson AL, Tutt A, Lonning PE, and Campbell PJ (2017). Genomic evolution of breast cancer metastasis and relapse. Cancer Cell 32, 169–184.e167. [PubMed: 28810143]

Yu G, Wang LG, Han Y, and He QY (2012). clusterProfiler: an R package for comparing biological themes among gene clusters. OMICS 16, 284–287. [PubMed: 22455463]

Yu G, Wang LG, and He QY (2015). ChIPseeker: an R/Bioconductor package for ChIP peak annotation, comparison and visualization. Bioinformatics 31, 2382–2383. [PubMed: 25765347]

Zhang Y, Liu T, Meyer CA, Eeckhoute J, Johnson DS, Bernstein BE, Nusbaum C, Myers RM, Brown M, Li W, and Liu XS (2008). Model-based analysis of ChIP-Seq (MACS). Genome Biol. 9, R137. [PubMed: 18798982]

Zhu LJ, Gazin C, Lawson ND, Pagès H, Lin SM, Lapointe DS, and Green MR (2010). ChIPpeakAnno: a Bioconductor package to annotate ChIP-seq and ChIP-chip data. BMC Bioinformatics 11, 237. [PubMed: 20459804]

Zhu K, Liang W, Ma Z, Xu D, Cao S, Lu X, Liu N, Shan B, Qian L, and Yuan J (2018). Necroptosis promotes cell-autonomous activation of pro-inflammatory cytokine gene expression. Cell Death Dis. 9, 500. [PubMed: 29703889]

Highlights

- Recurrent tumors show global changes in gene expression and histone modifications
- Recurrent tumors are dependent on activity of the histone methyltransferase G9a
- G9a represses pro-inflammatory genes in recurrent tumors
- G9a inhibition in recurrent tumors leads to induction of necroptotic cell death

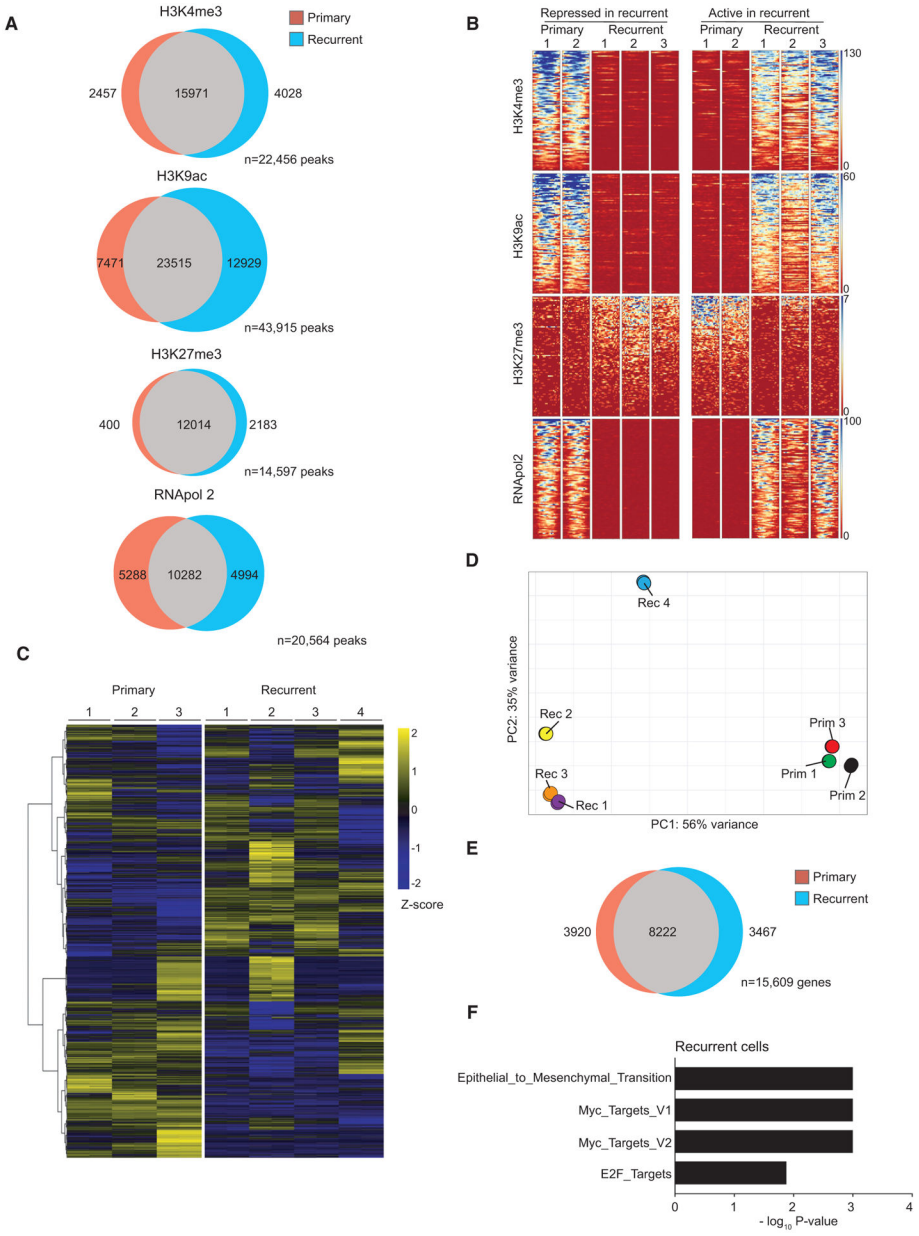

Figure 1. Tumor Recurrence Is Associated with Widespread Epigenetic Remodeling

(A) Venn diagrams showing the number of ChIP-seq peaks unique to primary (n = 2, biologically independent cell lines) or recurrent (n = 3, biologically independent cell lines) tumor cells, and the total number of peaks analyzed for each epigenetic mark.

(B) Heatmaps showing enrichment for active (H3K4me3 and H3K9ac) and repressive (H3K27me3) histone marks at the top 100 differentially RNApol2-bound genes in primary (left) and recurrent (right) tumor cell lines. Each row represents a different gene promoter. n = 2, biologically independent primary cell lines, and n = 3, biologically independent recurrent cell lines.

(C) Heatmaps showing unsupervised hierarchical clustering of 15,609 genes analyzed by RNA-seq for three independent primary and four independent recurrent tumor cell lines.

Sequencing was performed in duplicate for each cell line. Genes were median centered and *Z* score normalized within rows.

(D) Principal components analysis (PCA) of RNA-seq from (C).

(E) Venn diagram showing the number of differentially expressed genes (adj. $p < 0.05$) between primary and recurrent tumor cell lines.

(F) Gene set enrichment analysis showing significantly enriched pathways in recurrent tumor cells. For (D) and (E), n = 3, biologically independent primary cell lines, and n = 4, biologically independent recurrent cell lines.

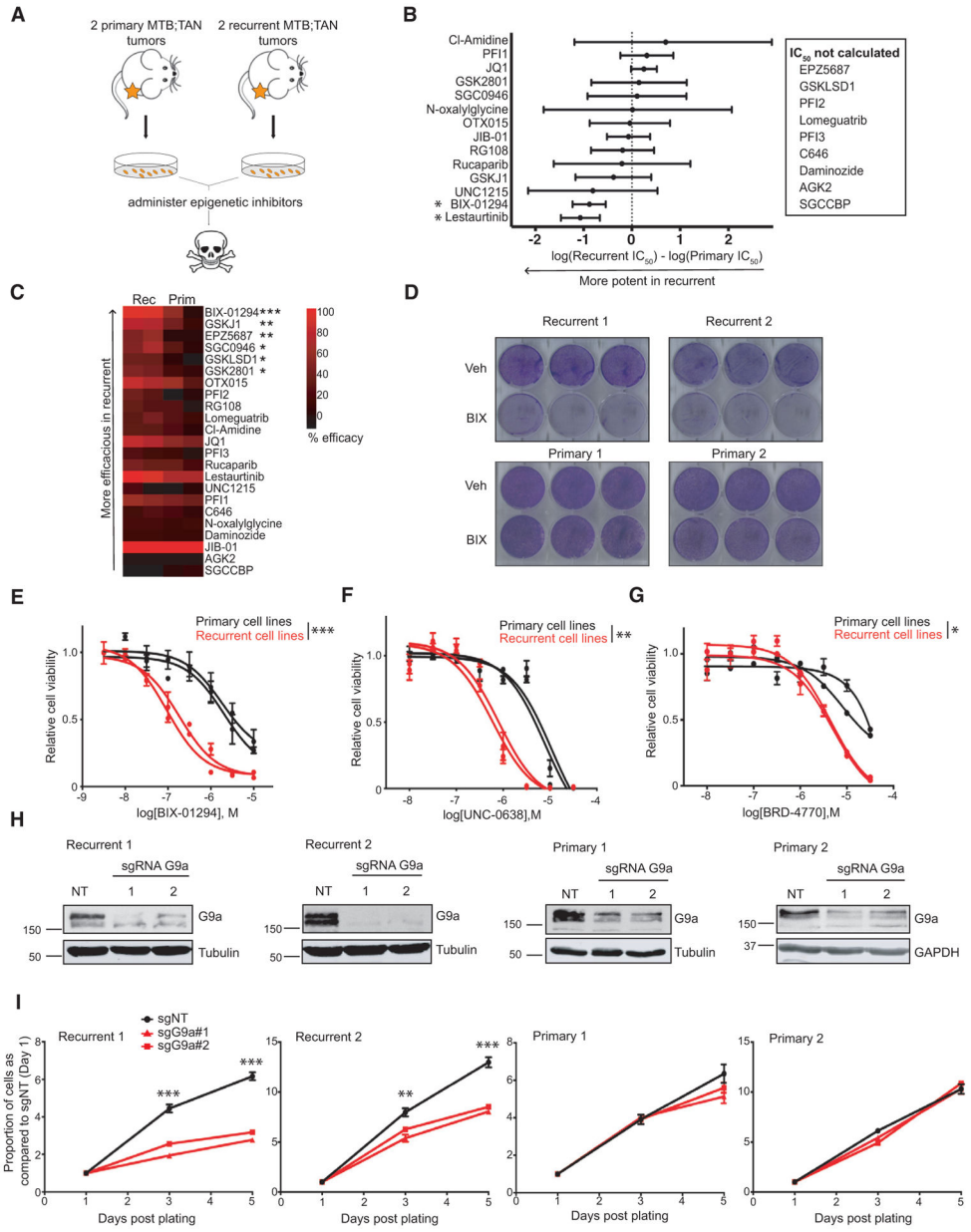

Figure 2. Recurrent Tumors Are Dependent upon G9a Histone Methyltransferase Activity

(A) Tumor cells derived from primary or recurrent MTB/TAN tumors were treated with a panel of small-molecule inhibitors targeting epigenetic enzymes.

(B) Forest plot showing the difference in IC_{50} between recurrent and primary tumor cells for each epigenetic inhibitor. Differences in IC_{50} values are shown with 95% confidence intervals. n = 2, biologically independent primary cell lines, and n = 2, biologically independent recurrent cell lines.

(C) Heatmaps showing the efficacy of each tested drug at the lowest concentration producing maximal cell growth inhibition. Significance between drug efficacy was determined by two-way ANOVA (drug × cohort) and Sidak's multiple comparison test. n = 2, biologically independent primary cell lines, and n = 2, biologically independent recurrent cell lines.

(D) Crystal violet staining of primary or recurrent tumor cells treated with vehicle or 2 μM BIX-01294 for 48 h. n = 2, biologically independent primary cell lines, and n = 2, biologically independent recurrent cell lines.

(E–G) Concentration response curves for primary (black) and recurrent (red) tumor cells treated with increasing concentrations of BIX-01294 (E), UNC-0638 (F), or BRD-4770 (G). IC_{50} and standard error values were calculated for each cohort by non-linear regression and significance was evaluated by Student's unpaired t test. Data are shown for two biologically independent primary cell lines and two biologically independent recurrent cell lines, and for each cell line, three technical replicates were measured.

(H) Western blot analysis for G9a expression after infection with one of two independent sgRNAs targeting G9a (sgG9a#1 or sgG9a#2) or a non-targeting sgRNA (sgNT) in Cas9-expressing primary and recurrent tumor cell lines.

(I) Growth curves for control and G9a-knockdown primary and recurrent tumor cells. Asterisks denote significance between control and the nearest G9a sgRNA. Significance was determined by two-way ANOVA (time × sgRNA) followed by Sidak's multiple comparison test. Data are shown for two biologically independent primary cell lines and two biologically independent recurrent cell lines, and for each cell line, three technical replicates were measured.

Error bars denote means ± SEM. *$p < 0.05$, **$p < 0.01$, ***$p < 0.001$.

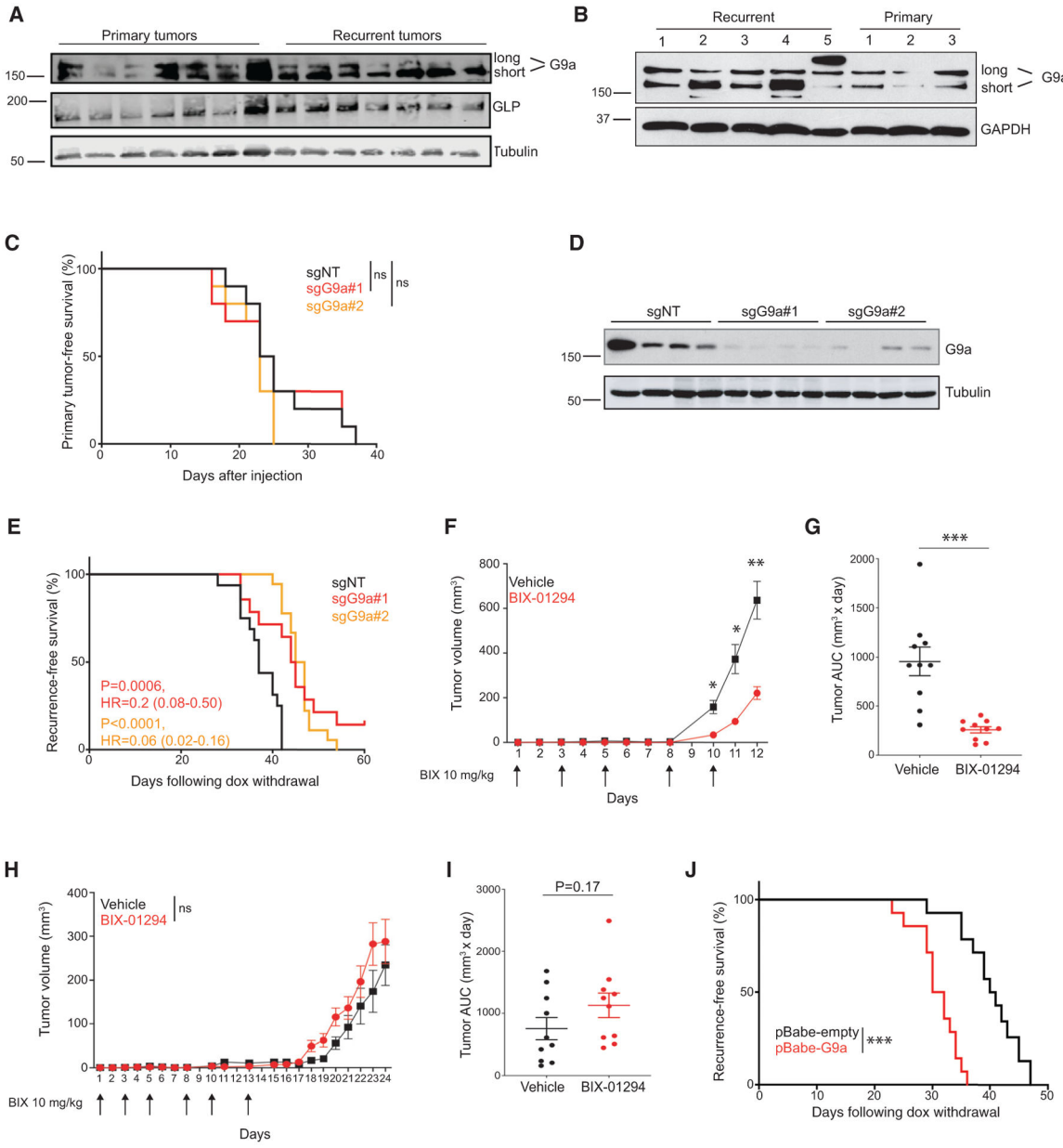

Figure 3. G9a Promotes Tumor Recurrence *In Vivo*

(A) Western blot analysis for G9a expression in seven biologically independent primary and seven biologically independent recurrent MTB;TAN tumors. Quantification of each G9a isoform is shown relative to primary tumor #1.

(B) Western blot analysis for G9a expression in three biologically independent primary and five biologically independent and recurrent tumor-derived cell lines. Quantification of each G9a isoform is shown relative to primary cell line #1.

(C) Kaplan-Meier survival curves showing time until primary tumor formation (~75 mm^3) for mice injected orthotopically with sgNT-, sgG9a#1-, or sgG9a#2- expressing primary tumor cells (primary #2: n = 10 mice [20 tumors] per cohort). Statistical significance was determined by Mantel-Cox log-rank test.

(D) Western blot analysis of G9a expression in representative primary tumors from panel (C).

(E) Kaplan-Meier survival curves showing recurrence-free survival for sgNT-, sgG9a#1-, or sgG9a#2-expressing tumors. p Values, hazards ratios, and 95% confidence intervals are indicated as compared with sgNT. n = 8 mice (16 tumors) per cohort. Statistical significance was determined by Mantel-Cox log-rank test.

(F) Mean tumor growth curves for recurrent tumor cell line #3 injected bilaterally into the mammary gland of FVB mice (n = 10 tumors/cohort) and treated with vehicle or 10 mg/kg BIX-01294 three times a week. Arrows indicate drug treatments. Significance was determined by repeated-measures two-way ANOVA (time × treatment) with Sidak's post hoc test.

(G) Area under the curve (AUC) values for tumor growth curves shown in (F). Significance was determined by Student's unpaired t test.

(H) Mean tumor growth curves for primary tumor cell line #2 injected bilaterally into the mammary gland of TAN mice (n = 10 tumors/cohort) and treated with vehicle or 10 mg/kg BIX-01294 three times a week for 2 weeks. Arrows indicate drug treatments. Significance was determined by repeated-measures two-way ANOVA (time × treatment) with Sidak's post hoc test.

(I) AUC values for tumor growth curves shown in (H). Significance was determined by Student's unpaired t test.

(J) Kaplan-Meier survival curves showing recurrence-free survival for control or G9a-overexpressing tumors. n = 7 mice (14 tumors) per cohort. Statistical significance was determined by Mantel-Cox log-rank test.

Results from (A) are representative of three independent experiments. Results from (B) are representative of two independent experiments. Error bars denote means ± SEM. *$p < 0.05$, **$p < 0.01$, ***$p < 0.001$.

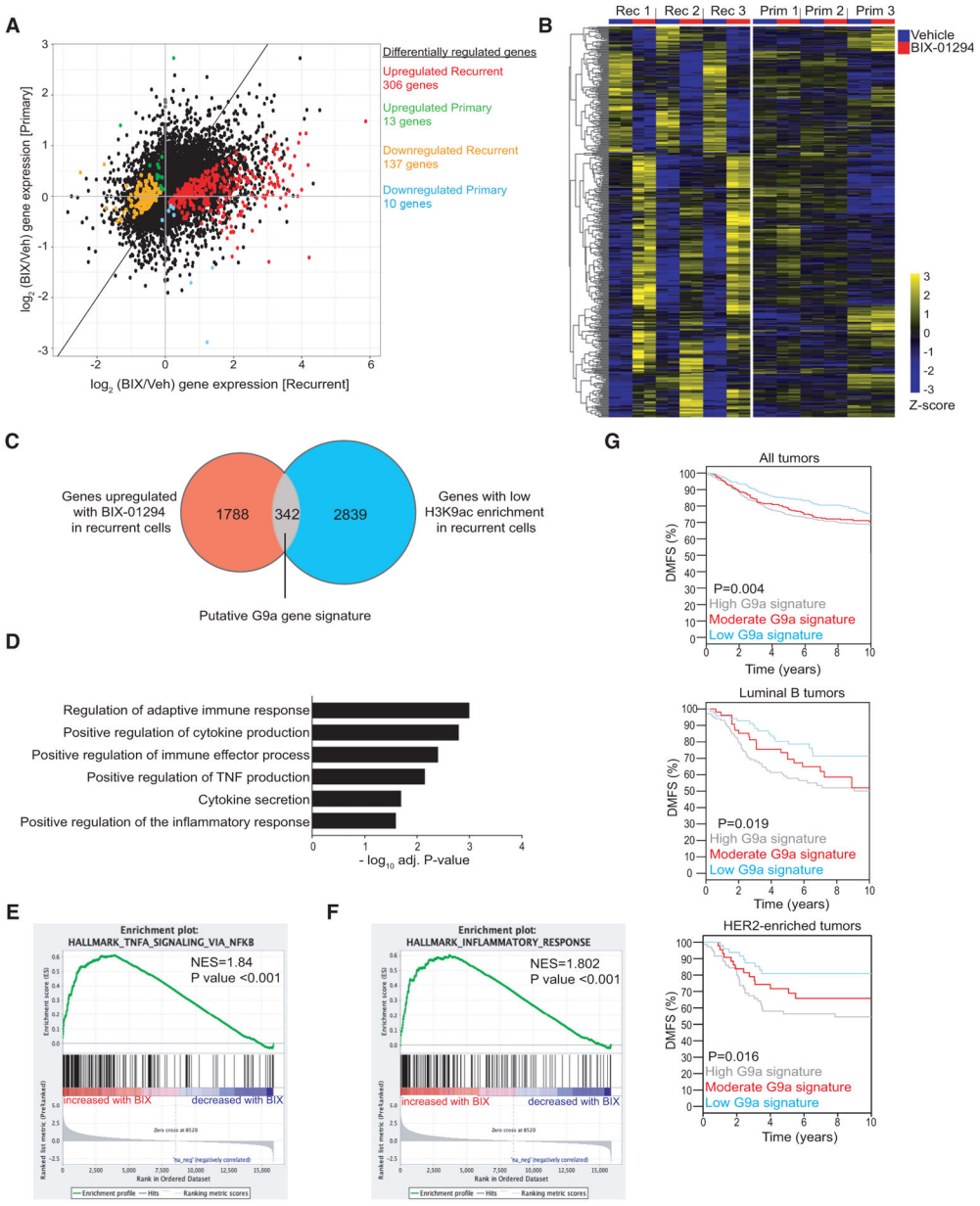

Figure 4. Integrated Epigenetic and Transcriptional Analysis of G9a-Regulated Genes in Recurrent Tumors

(A) Comparison of gene expression changes 16 h after BIX-01294 (1 μM) treatment in recurrent (x axis) and primary (y axis) tumor cells. Colored dots indicate genes whose expression was differentially regulated by BIX treatment in primary versus recurrent tumor cells (adj. $p < 0.05$). Sequencing was performed on three biologically independent primary cell lines, and n = 3, biologically independent recurrent cell lines in duplicate for each cell line.

(B) Heatmaps showing median-centered, *Z*-score-normalized expression changes for differentially genes from (A).

(C) A G9a gene signature was generated by overlapping genes upregulated following BIX-01294 treatment in recurrent tumor cells (adj. $p < 0.05$) with genes whose promoters had significantly lower H3K9ac in recurrent tumor cells (adj. $p < 0.05$).
(D) Gene ontology analysis showing pathways enriched in the 342 gene G9a signature from (C).
(E and F) GSEA plots showing enrichment of a TNF/NF-κB signature (F) and an inflammatory signature (G) in recurrent tumor cells after G9a inhibition.
(G) Kaplan-Meier plots showing distant metastasis-free survival (DMFS) for all tumors (n = 1,379), HER2-enriched tumors (n = 105), and luminal B tumors (n = 225) in patients stratified by high (gray), moderate (red), or low (blue) expression of G9a signature genes.

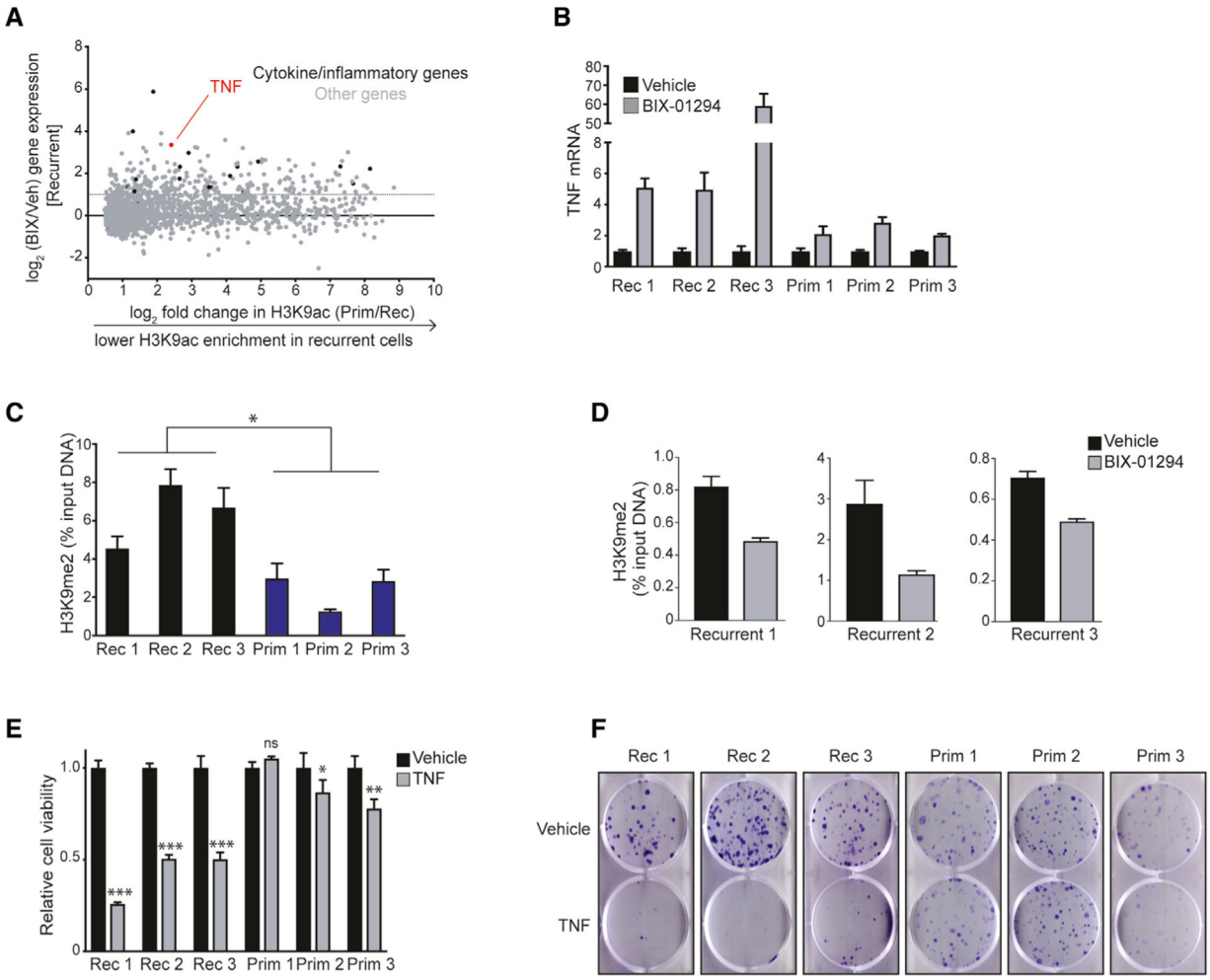

Figure 5. G9a-Dependent Silencing of TNF Is Required for Recurrent Tumor Cell Survival

(A) Scatterplot showing genes induced after BIX-01294 treatment in recurrent tumor cells (y axis) as a function of differential H3K9ac peaks in recurrent tumor cells (x axis). Dashed line indicates two-fold mRNA upregulation. Inflammatory genes identified from the G9a-regulated gene set are indicated in black.

(B) qPCR analysis for TNF expression 16 h after BIX-01294 treatment (1 μM) in three biologically independent recurrent tumor cell lines and three independent primary tumor cell lines. Expression values were normalized to the vehicle within each cell line.

(C) ChIP-qPCR showing H3K9me2 enrichment at the TNF promoter in three biologically independent recurrent tumor cell lines and three independent primary tumor cell lines

(D) ChIP-qPCR showing H3K9me2 enrichment at the TNF promoter in three biologically independent recurrent cell lines following 16 h of 1 μM BIX-01294 treatment. Two replicates were performed for each cell line.

(E) Cell viability of primary and recurrent tumor cells treated with TNF (10 ng/mL) for 3 days. Data are shown for three biologically independent primary cell lines and three biologically independent recurrent cell lines, and three technical replicates were measured for each cell line. Significance was determined by one-way ANOVA and Tukey's post hoc test.

(F) Representative colony formation assays showing viability of primary and recurrent tumor cells after 7-day treatment with TNF (10 ng/mL). Data are shown for three biologically independent primary cell lines and three biologically independent recurrent cell lines.

Results from panels (E) and (F) are representative of at least two independent experiments. Error bars denote means ± SEM. *p < 0.05, **p < 0.01, ***p < 0.001, ns = not significant.

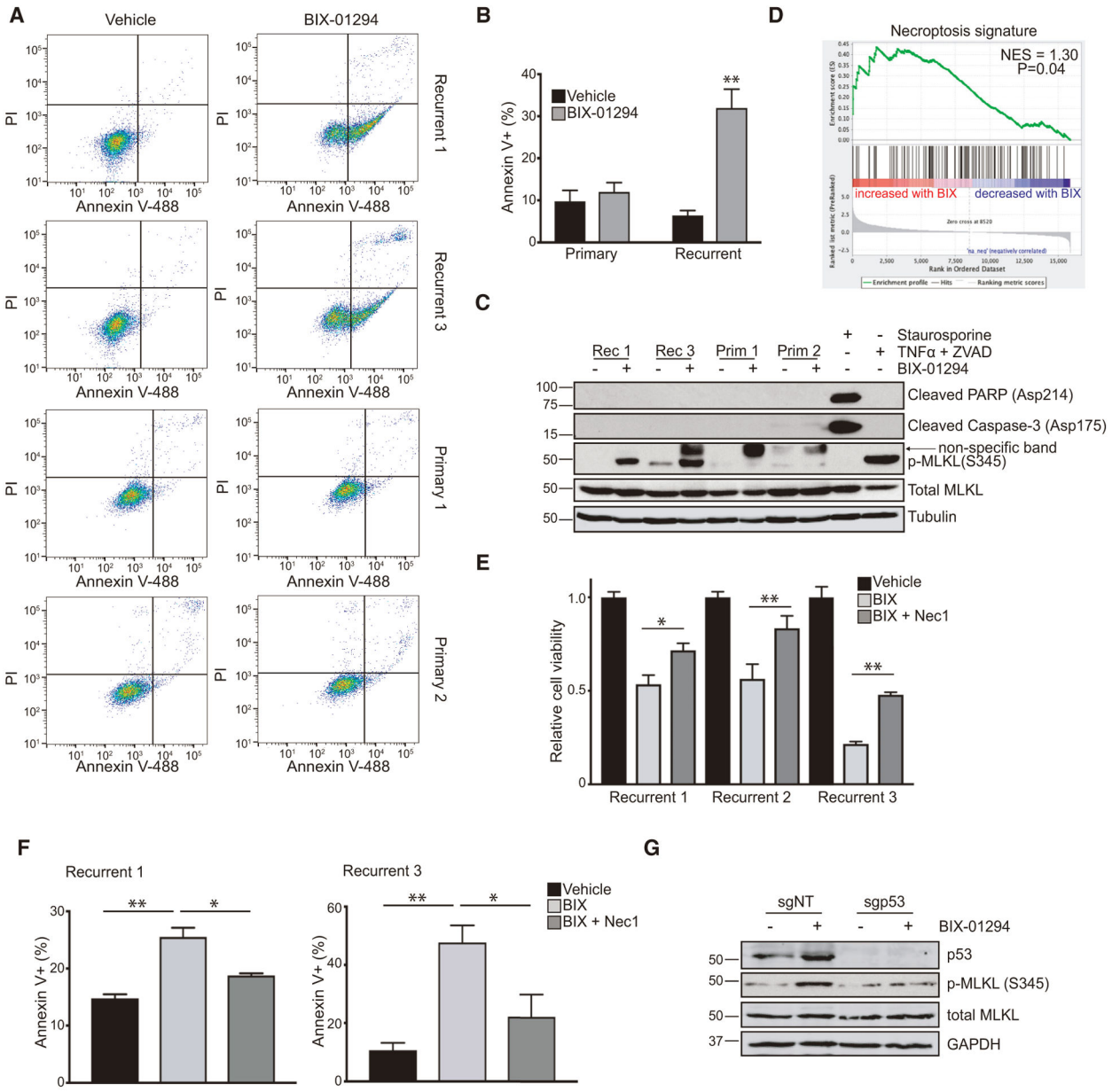

Figure 6. G9a Inhibition Induces Necroptotic Cell Death in Recurrent Tumors

(A) Annexin V/PI staining of two biologically independent primary cell lines and two biologically independent recurrent cell lines treated with vehicle or 1 μM BIX-01294 for 16 h.

(B) Quantification of Annexin V-positive cells from (A). Significance was determined by one-way ANOVA and Tukey's post hoc test.

(C) Western blot analysis for cleaved PARP (Asp214), cleaved Caspase-3 (Asp175), p-MLKL (S345), and total MLKL in recurrent and primary tumor cells treated with vehicle or 1 μM BIX-01294. Staurosporine and TNF + Z-VAD-FMK were included as controls for apoptosis and necroptosis, respectively.

(D) GSEA showing enrichment of a curated necroptosis signature in recurrent tumor cells treated with BIX-01294. p value and normalized enrichment score are shown.
(E) Cell viability of three biologically independent recurrent tumor cells after 16-h treatment with BIX-01294 (300 nM) alone or in combination with necrostatin-1 (30 μM). Three technical replicates were measured for each cell line.
(F) Quantification of Annexin V staining in two biologically independent recurrent tumor cell lines treated for 24 h with BIX-01294 (750 nM) alone or in combination with necrostatin-1 (30 μM). Three technical replicates were measured for each cell line. Significance in (E) and (F) was determined by one-way ANOVA with Tukey's post hoc test.
(G) Western blot analysis showing p53, p-MLKL (S345), and total MLKL in control or p53-knockout recurrent tumor cells (#3) treated with vehicle or16 h with 1 μM BIX-01294.
Results from (A)–(C) and (E)–(G) are representative of at least two independent experiments. Error bars denote means ± SEM. *$p < 0.05$, **$p < 0.01$, ns = not significant.

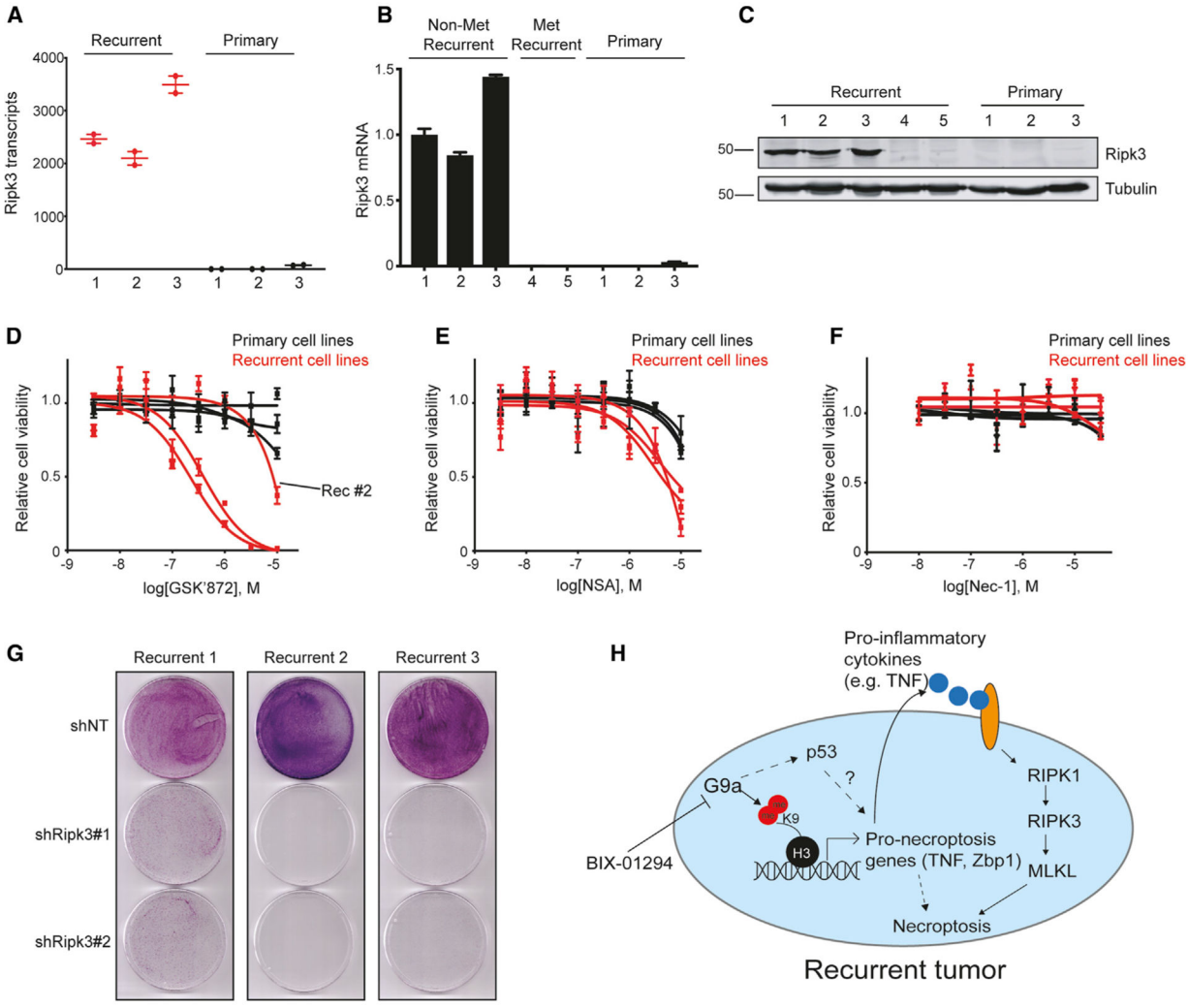

Figure 7. Recurrent Tumors Are Dependent on RIPK3

(A) RNA transcript counts for RIPK3 in three biologically independent recurrent tumor cells and three biologically independent primary tumor cells as determined by RNA-seq analysis.

(B) qPCR showing RIPK3 expression in three biologically independent non-Met-amplified recurrent tumor cells, two biologically independent Met-amplified recurrent tumor cells, and three biologically independent primary tumor cells.

(C) Western blot analysis for RIPK3 expression in primary and recurrent tumor cells.

(D–F) Concentration-response curves for primary and recurrent tumor cells treated with increasing doses of GSK'872 (D), Necrosulfonamide (E), and Necrostatin-1 (F). Data are shown for three biologically independent primary cell lines and three biologically independent recurrent cell lines, and for each cell line, three technical replicates were measured.

(G) Cell viability after genetic knockdown of RIPK3 with two independent shRNAs or a scrambled control shRNA in three biologically independent recurrent tumor cell lines.

(H) RIPK3-driven recurrent tumors require G9a activity to silence pro-inflammatory and pro-necroptotic gene expression and prevent necroptosis. Error bars denote means ± SEM.

KEY RESOURCES TABLE

REAGENT or RESOURCE	SOURCE	IDENTIFIER
Antibodies		
H3K9me2 Rabbit (WB 1:1000)	Cell Signaling	Cat#4658; RRID: AB_10544405
Histone 3 Mouse (WB 1:1000; ICW 1:500)	Cell Signaling	Cat#3638; RRID: AB_1642229
G9a Rabbit (WB 1:1000)	Cell Signaling	Cat#3306; RRID: AB_2097647)
GAPDH Mouse (WB 1:2000)	Santa Cruz	Cat#8795; RRID: AB_1078991
Tubulin Mouse (WB 1:2000)	Cell Signaling	Cat#3873; RRID: AB_1904178
P53 Mouse (WB 1:1000)	Cell Signaling	Cat#2524; RRID: AB_331743
Cleaved PARP Rabbit (WB 1:1000)	Cell Signaling	Cat#9544; RRID: AB_2160724
Cleaved Caspase Rabbit (WB 1:1000)	Cell Signaling	Cat#9661; RRID: AB_2341188
MLKL Rabbit (WB 1:1000)	Cell Signaling	Cat#37705; RRID: AB_2799118
p-MLKL Rabbit(S345) (WB 1:1000)	Abcam	Cat#196436; RRID: AB_2687465
RIPK3 Mouse (WB 1:500)	Santa Cruz	Cat#374639; RRID: AB_10992232
H3K9me2 Rabbit (ChIP 5 μg; ICW 1:500)	Abcam	Cat#1220; RRID: AB_449854
H3K9ac Rabbit(ChIP 5 μg)	Abcam	Cat#4441; RRID: AB_2118292
H3K4me3 Rabbit (ChIP 5 μg)	Abcam	Cat#8580; RRID: AB_306649
H3K27me3 Rabbit (ChIP 5 μg)	Abcam	Cat#6002; RRID: AB_305237
RNApol II CTD Repeat YSPTSPS Rabbit (ChIP 5 ug)	Abcam	Cat#817; RRID: AB_306327
Mouse IgG isotype control (ChIP 5 ug)	Abcam	Cat#18392
Rabbit IgG isotype control (ChIP 5 ug)	Abcam	Cat#171870; RRID: AB_2687657
Goat anti-rabbit IgG (H + L)-HRP	Biorad	Cat#1706515; RRID: AB_11125142
CD11-PE (FACS 1:50)	BD Biosciences	Cat#561689; Clone M1/70; RRID: AB_10893803
F4/80 - AF687 (FACS 1:50)	BD Biosciences	Cat#565853; Clone T452341; RRID: AB_2744474
CD3e-PE (FACS 1:100)	BD Biosciences	Cat#561824; Clone1452C11; RRID: AB_10898340
CD8a-APC (FACS 1:200)	BD Biosciences	Cat#561093; Clone 536.7; RRID: AB_10563416
CD4-APCCy7 (FACS 1:100)	BD Biosciences	Cat#561830; clone GK1.5; RRID: AB_10897172
CD45-APC (FACS 1:100)	BD Biosciences	Cat#561018; clone 30-F11; RRID: AB_10584326
CD16/CD32	Invitrogen	Cat#14-0161-82; RRID: AB_467133
AlexaFluor 680 (WB 1:5000)	ThermoFisher	Cat#A21076; RRID: AB_2535736
IRDye 800 (WB 1:5000)	Li-Cor	Cat#92632210; RRID: AB_621842
Chemicals, Peptides, and Recombinant Proteins		
BIX-01294	Tocris	Cat# 3364
UNC0638	Tocris	Cat# 4343
BRD4770	SelleckChem	Cat# S7591
Nec-1	SelleckChem	Cat#S8037
GSK126	SelleckChem	Cat#S7061
Necrosulfonamide	SelleckChem	Cat#S8251

REAGENT or RESOURCE	SOURCE	IDENTIFIER
Recombinant mTNF	Biolegend	Cat#575202
Z-VAD-FMK	SelleckChem	Cat#S7023
Epigenetics screening library (including Cl⁻Amidine, PFI-1, JQ1, GSK2801, SGC0946, N-oxalylglycine, OTX015, JIB01, RG108, Rucaparib, GSKJ1, UNC1215, lestaurtinib, BIX-01294, EPZ5687, GSKLSD1, PFI2, Lomeguatrib, PFI3, C646, Daminozide, AGK2, SGCCBP)	CaymanChem	Cat #11076
Polybrene	Sigma	Cat#107689
Puromycin	Sigma	Cat#P8833
Blasticidin	GIBCO	Cat#A11139–03
Collagenase / hyaluronidase	Stemcell	Cat#7912
Dispase	Stemcell	Cat#7913
DNase I	Worthington Biochemical	Cat#LS002006
FBS	Corning	Cat#35010CV
Penicillin/Streptomycin	Gicbo	Cat#15140–122
Doxycycline	RPI	Cat#D43020
Critical Commercial Assays		
CellTiterGLO	Promega	Cat#G7571
AllPrep kit	QIAGEN	Cat#80204
RNAeasy kit	QIAGEN	Cat#74104
Taqman master mix solution	Applied Biosystems	Cat#4369016
Dead cell apoptosis kit with Annexin V AlexaFluor 488 nm & propidium iodide	ThermoFisher Scientific	Cat#V13241
Deposited Data		
ChIP-sequencing for H3K27me3, H3K4me3, H3K9ac, RNApol 2	This paper	PRJNA505839
RNA-sequencing for vehicle and BIX-01294 treatment in primary lines (#1, #2, #3) and recurrent line (#1, #2, #3, #4)	This paper	PRJNA505839
Experimental Models: Cell Lines		
Primary #1 (Internal 54074)	This lab	
Primary #2 (Internal 99142)	This lab	
Primary #3 (Internal 216942)	This lab	
Recurrent #1 (Internal 42929)	This lab	
Recurrent #2 (Internal 48316)	This lab	
Recurrent #3 (Internal 20342)	This lab	
Recurrent#4 (Internal 40977)	This lab	
Recurrent#5 (Internal 1669)	This lab	
Human SKBR3	Duke Cell Culture Facility	RRID:CVCL_0033
Human AU565	Duke Cell Culture Facility	RRID:CVCL_1074
Human BT-474	Duke Cell Culture Facility	RRID:CVCL_0179
Human HCC1500	Duke Cell Culture Facility	RRID:CVCL_1254
Human HCC1428	Duke Cell Culture Facility	RRID:CVCL_1253
Human T-47D	Duke Cell Culture Facility	RRID:CVCL_0553
Human MCF-7	Duke Cell Culture Facility	RRID:CVCL_0031
Human HCC1937	Duke Cell Culture Facility	RRID:CVCL_0290

REAGENT or RESOURCE	SOURCE	IDENTIFIER
Human HCC1143	Duke Cell Culture Facility	RRID:CVCL_1245
Human MDA-MB-231	Duke Cell Culture Facility	RRID:CVCL_0062)
Human MCF10A	Duke Cell Culture Facility	RRID:CVCL_0598
Human MDA-MB-468	Duke Cell Culture Facility	RRID:CVCL_0419
Human HCC202	Duke Cell Culture Facility	RRID:CVCL_2062
Human MDA-MB-134	Duke Cell Culture Facility	RRID:CVCL_0617
Human HCC1395	Duke Cell Culture Facility	RRID:CVCL_1249
Human MDA-MB-361	Duke Cell Culture Facility	RRID:CVCL_0620
Human HCC38	Duke Cell Culture Facility	RRID:CVCL_1267
Human BT-483	Duke Cell Culture Facility	RRID:CVCL_2319
Human HCC1954	Duke Cell Culture Facility	RRID:CVCL_1259
Human MDA-MB-436	Duke Cell Culture Facility	RRID:CVCL_0623
Human BT-549	Duke Cell Culture Facility	RRID:CVCL_1092
Human HCC1569	Duke Cell Culture Facility	RRID:CVCL_1255
Human ZR-75–1	Duke Cell Culture Facility	RRID:CVCL_0588
Human UACC-812	Duke Cell Culture Facility	RRID:CVCL_1781
Human BT-20	Duke Cell Culture Facility	RRID:CVCL_0178
Human MDA-MB-157	Duke Cell Culture Facility	RRID:CVCL_0618
Human HCC1419	Duke Cell Culture Facility	RRID:CVCL_1251
Human HS578T	Duke Cell Culture Facility	RRID:CVCL_0332
Experimental Models: Organisms/Strains		
MMTV-rtTA;TetO-Her2/neu (MTB;TAN) on FVB	Lewis Chodosh	
TetO-Her2/neu (TAN) on FVB	Lewis Chodosh	
FVB mice	Jackson laboratories	
Nu/nu female mice	Duke University Breeding Core	
Oligonucleotides		
G9a cDNA overexpression plasmid generation Forward: 5′-GTTAGGA TCCATGGCGGCGGCGGCGGGAGC-3′	This paper	N/A
G9a cDNA overexpression plasmid generation Reverse: 5′-GTTAGAATT CTTAAGAGTCCTCAGGT GTTG-3′.	This paper	N/A
sgG9a#1: 5’-CGGCAGGCTCCAAG GAGTCG-3’	This paper	N/A
sgG9a#2: 5’-ACAGGCACCCCC CTTGCTGG-3’	This paper	N/A
sgNT: 5′-CCCGATCCCC TACCTAGCCG-3′	This paper	N/A
sgP53: 5’-GAAGTCACAGCACATGA CGG-3’	This paper	N/A
shRNA scrambled control	Addgene	Cat#1864
shRNA Ripk3#1	Dharmacon	TRCN0000022534
shRNA Ripk3#2	Dharmacon	TRCN0000022538
Primers used for H3K9me2 ChIP-qPCR see Table S5	This paper	
Taqman Cdkn1a probe	ThermoFisher Scientific	Cat#Mm00432448
Taqman Ehmt2 probe	ThermoFisher Scientific	Cat#Mm01132261
Taqman Tnf (mouse) probe	ThermoFisher Scientific	Cat#Mm00443258
Taqman Ripk3 (mouse) probe	ThermoFisher Scientific	Cat#Mm00444947
Taqman Actb probe	ThermoFisher Scientific	Cat#Mm02619580

REAGENT or RESOURCE	SOURCE	IDENTIFIER
Taqman 18 s (Mouse and Human) probe	ThermoFisher Scientific	Cat#4332641
Taqman Gadd45a probe	ThermoFisher Scientific	Cat#Mm00432802
Taqman Met probe	ThermoFisher Scientific	Cat#Mm01156972
Taqman TNF (Human) probe	ThermoFisher Scientific	Cat#Hs00174128
Taqman RIPK3 (Human) probe	ThermoFisher Scientific	Cat#Hs01011175
Taqman copy number Met probe	ThermoFisher Scientific	Cat#Mm00565151
Taqman copy number tnfr probe	ThermoFisher Scientific	Cat#4458366
Recombinant DNA		
Lenti-Cas9-blast	Addgene	Cat#52962
Lentiguide-puro	Addgene	Cat#52963
Full-length G9a cDNA	Dharmacon	Clone ID: 6822432
psPAX2	Addgene	Cat#12260
pMDG.2	Addgene	Cat#12559
pBABE-puro	Addgene	Cat#1764
Software and Algorithms		
Bowtie	Langmead et al., 2009	
MACS2	Feng et al., 2012	https://pypi.org/project/MACS2/
Diffbind	Ross-Innes et al., 2012	https://bioconductor.org/packages/release/bioc/html/DiffBind.html
ChIPseeker	Yu etal., 2015	http://bioconductor.org/packages/release/bioc/html/ChIPseeker.html
annotatr	Cavalcante and Sartor, 2017	https://bioconductor.org/packages/release/bioc/html/annotatr.html
Deeptools2	Ramírez, et al., 2016	https://deeptools.readthedocs.io/en/develop/content/installation.html
ChIPpeakAnno	Zhu etal., 2010	https://www.bioconductor.org/packages/release/bioc/html/ChIPpeakAnno.html
IGV desktop viewer (v2.3)	Broad Institute	http://software.broadinstitute.org/software/igv/
ENCODE for H3K27ac and H3K4me1 in mouse fibroblasts	Bing Ren from the ENCODE consortium	GSM1000139; GSM769028
Rsubread	Liao et al., 2019	http://subread.sourceforge.net/
pheatmap		https://cran.r-project.org/web/packages/pheatmap/index.html
clusterProfiler	Yu etal., 2012	https://bioconductor.org/packages/release/bioc/html/clusterProfiler.html
GSEA desktop viewer (v4.0)	Broad Institute	https://www.gsea-msigdb.org/gsea/index.jsp
DESeq2	Love et al., 2014	https://bioconductor.org/packages/release/bioc/html/DESeq2.html
Confidence Interval for IC_{50} calculator	GraphPad	Available from:https://www.graphpad.com/quickcalcs/errorProp1/?Format=SEM
ImageStudio Lite (v5.0)	Li-Cor	https://www.licor.com/bio/image-studio-lite/
FlowJo (v10)	FlowJo	
Prism 7	Graphpad	